Geochemistry 85 (2025) 126351

Contents lists available at ScienceDirect

Geochemistry

journal homepage: www.elsevier.com/locate/chemer

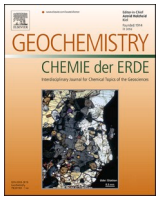

Ediacaran and early-palaeozoic bimodal volcanism in the Ossa-Morena Zone, SW Iberian Massif: New clues for intraplate rifting shortly after the Cadomian Orogeny

P. Cachapuz [a,*], M. Chichorro [b], T. Bento dos Santos [a,c], D.R. Carvalho [d], U. Linnemann [e], M. Zieger-Hofmann [e], J. Zieger [e], E. Dantas [f], R.V. Santos [f], P. Moita [g], M. Beltrame [g], A.R. Solá [d], M. Díaz-Azpíroz [h], C. Fernández [i]

[a] *Instituto Dom Luiz (IDL), Faculdade de Ciências, Universidade de Lisboa, Campo Grande, 1749–016, Lisboa, Portugal*
[b] *FCT-UNL - Faculdade de Ciências e Tecnologia, Universidade Nova de Lisboa, 2829-516, Caparica, Portugal*
[c] *DG-FCUL – Departamento de Geologia, Faculdade de Ciências, Universidade de Lisboa, Campo Grande, 1749-016, Lisboa, Portugal*
[d] *LNEG – Laboratório Nacional de Energia e Geologia, 2720-866, Amadora, Portugal*
[e] *Senckenberg Naturhistorische Sammlungen Dresden, Museum für Mineralogie und Geologie, Königsbrücker Landstr. 159, 01109, Dresden, Germany*
[f] *LEGGA - Laboratório de Geocronologia, Instituto de Geociências, Universidade de Brasília (UnB), Brazil*
[g] *HERCULES Laboratory, In2Past, Associated Laboratory, Geosciences Department, School of Sciences and Technology, University of Évora, Rua do Cardeal Rei, s/n, 7000-849, Évora, Portugal*
[h] *Departamento de Sistemas Físicos, Químicos y Naturales, Universidad Pablo de Olavide, Seville, Spain*
[i] *Departamento de Geodinámica y Paleontología, Universidad de Huelva, Campus del Carmen, 21071, Huelva, Spain*

ARTICLE INFO

Handling Editor: Federico Lucci

Keywords:
SW Iberia
Meta-volcanic rocks
Rheic
Geochemistry
Rifting

ABSTRACT

This study focuses on bimodal meta-volcanic rocks present in the Iberian Massif, in the Évora-Aracena Metamorphic Belt of the Ossa-Morena Zone (OMZ), near the boundary with the South Portuguese Zone. New petrological, geochemical (whole-rock and Sr—Nd isotopes) and LA-ICP-MS U—Pb zircon geochronology data are presented to track the magmatic evolution of both felsic and mafic rocks and their respective geodynamic setting during the transition between the Cadomian Orogeny and subsequent Palaeozoic rifting events.

Our research shows that the Évora-Aracena Metamorphic Belt (EAMB) in the southwestern OMZ possesses a significant record of the transition between the Cadomian and Variscan cycles. U—Pb geochronological data confirm the existence of both felsic and mafic Ediacaran igneous rocks (546 and 556 Ma, respectively), a novelty in the region. The Cadomian-related felsic rocks show geochemical similarities to meta-felsic rocks formed during the initial phases of the Cambrian rifting event, namely very negative εNd values (−10.1 to −11.8), depleted HREE patterns and orogenic signatures. Such similarities imply that meta-felsic rocks formed in the earliest stages of the Cambrian Rift-to-Drift event resulted from a shallower melting.

Moreover, meta-felsic rocks formed in the early stages of the Cambrian rifting (525 Ma) present a significant amount of Ediacaran aged zircons, whereas the Cadomian-related counterparts display a few discordant Cambrian ages, likely a consequence of Pb-loss. This indicates that the convergent, subduction-related regime that prevailed during most of the Cryogenian-Ediacaran times along the boundaries of NW Gondwana was swiftly supplanted by a rift-dominated regime during the Cambrian, with no substantial gap between these two thermal events. Meanwhile, meta-felsic rocks formed during the Rift-to-Drift (525–480 Ma) event exhibit progressively higher εNd values (−5.0 to +3.0), HREE-enrichment, as well as anorogenic signatures, denoting an increasing contribution of mantle-derived melts. This increasing mantle contribution eventually led to the occurrence of bimodal magmatism in the Middle Cambrian Main Rift event. Such Cambrian mafic rocks, unlike the Ediacaran mafic rocks that present flat REE patterns and continental arc signatures, display varying degrees of LREE enrichment and N-MORB to *E*-MORB signatures.

* Corresponding author.
E-mail address: pedrofilipecachapuz@hotmail.com (P. Cachapuz).

https://doi.org/10.1016/j.chemer.2025.126351
Received 11 September 2025; Received in revised form 3 November 2025; Accepted 4 November 2025
Available online 9 November 2025

1. Introduction

The occurrence of bimodal volcanism is typically related to extensional geodynamic settings, such as continental rifting (e.g.: Mazzarini et al., 2004), back-arc lithospheric extension (e.g.: Shinjo and Kato, 2000) or post-collisional extensional regimes (e.g.: Bento dos Santos et al., 2015), although it has also been recognized in island or continental arcs (e.g.: Petrinovic et al., 2006). However, accurate correlation between each magmatic sequence and the several phases of a large global geodynamic event requires thorough geochemical studies, since geochemical characteristics are highly dependable on specific geological processes and tectonic setting (e.g.: Pearce et al., 1984). The use of robust geochemical data to decipher the geodynamic evolution of a particular region is, therefore, critical, particularly when such areas were later affected by large-scale tectono-metamorphic events, such as those related to the development of the largest collisional orogen of the Palaeozoic, the so-called Variscan-Alleghenian Orogeny (e.g.: Murphy et al., 2006) whose outcrops extend through North America, North Africa and Europe (Nance et al., 2008).

The presence of bimodal volcanic suites in the European portion of the Variscan orogen have long been identified in the Bohemian Massif, Massif Central, Armorican Massif, Eastern Pyrenees and the Ossa-Morena Zone (OMZ) in the SW Iberian Massif (e.g.: Dostal et al., 2001; Mata and Munha, 1990; Padel et al., 2018). The latter, together with the West Asturian-Leonese Zone (WALZ), Central Iberian Zone (CIZ) and the lower allochthonous units of the Galicia – Trás-os-Montes Zone (GTMZ) are typically interpreted as peripheric terrains the Gondwana palaeocontinent, on the dependence of an Ediacaran arc–back-arc system in transition to an early Palaeozoic continental Rift-to-Drift stage that led to the opening of the Rheic ocean (Quesada et al., 1990; Chichorro et al., 2008, 2022; Cotrim et al., 2021).

The opening of the Rheic ocean in the early Palaeozoic was responsible for the migration of peri-Gondwanan terranes, whereas its closure during the late Palaeozoic led to the Variscan-Alleghenian Orogeny and the formation of the supercontinent Pangea. According to some authors (Linnemann et al., 2007, 2008b), in the OMZ and in the Bohemian Massif, the rifting process responsible for the opening of the Rheic ocean was the extension of the Cadomian Orogeny (D'Lemos et al., 1990; Eguíluz et al., 2000; Linnemann et al., 2000; Murphy et al., 2002), since their genesis is highly dependent on the stretched Cadomian back-arc lithosphere (Linnemann et al., 2007, 2008a). Several aspects concerning the mechanisms underlying the opening of the Rheic ocean are still under discussion (e.g.:, Crowley et al., 2000; Hajná et al., 2018; Sánchez-García et al., 2010), specifically the relationship between the diachronic nature of the Cambrian-Ordovician Rift-to-Drift processes and the diachronic Ediacaran subduction as well as the potential oblique ridge-trench collision (Javier Álvaro et al., 2014, 2024). This is evidenced by the nature and timing of the magmatism recorded in the stratigraphy of the aforementioned peri-Gondwanan terranes (Nance et al., 2006; Sánchez-García et al., 2019).

The OMZ presents an extraordinary record of the late Neoproterozoic Cadomian magmatic arc and the oldest rifting events in the European Variscides, responsible for Rheic's formation (Eguíluz et al., 2000; Linnemann et al., 2007), making its study crucial for a better understanding of the tectono-magmatic processes that guided the transition from the Cadomian magmatic arc to the Variscan extensional setting and the formation of the Rheic ocean.

This work presents new petrological, geochemical (whole-rock and Sr—Nd isotopes) and LA-ICP-MS U—Pb zircon geochronology data of the bimodal volcanic rocks present in the Évora-Aracena Metamorphic Belt (EAMB; Fig. 1a and b), which is located in the SW sector of the OMZ, nearby the boundary with the South Portuguese Zone (SPZ). These volcano-sedimentary successions were formed during the transition between the Cadomian Orogeny and the Rift-to-Drift processes, having been later affected by strong Variscan tectonometamorphic imprint. Such imprint, although not sufficient to erase their primary geochemical and isotopic signatures, severely hampers its clear individualization, we believe that this new petrogenetic and geochronologic data is paramount to provide an excellent insight into the mechanisms involved in the early Palaeozoic rifting events.

2. Geological setting

The OMZ is a unique domain within the Iberian Massif, given the presence of a Neoproterozoic basement affected by the Cadomian Orogeny, overlapped by Palaeozoic lithologies (Quesada et al., 1990; Cachapuz et al., 2024). The protoliths of the Neoproterozoic metasediments ("Série Negra" Group) were deposited in a back-arc basin associated with the subduction of oceanic lithosphere under the western and northern margins of Gondwana (Eguíluz et al., 2000; Linnemann et al., 2008b). "Série Negra" Group essentially consist of metapelites and graphite-rich quartzwackes, at the bottom (Eguíluz, 1987), and a more detrital greywacke, with a volcanoclastic component, at the top (Quesada et al., 1990). The protoliths of the amphibolites and metagranitoids, formed during the Ediacaran, also outcrop within these metasedimentary units (Ábalos et al., 1991; Eguíluz et al., 2000; Mata and Munha, 1986).

The Cambrian units overlying the Neoproterozoic formations consist of a detrital-conglomeratic unit (Lower Detrital Series), succeeded by a detrital-carbonate sequence and a further detrital unit (Upper Detrital Series). This Neoproterozoic-Cambrian transition is marked by an angular discordance, signalling a shift from a collisional context to a continental rift setting (Sánchez-García et al., 2010, 2019). A rift system partitioned into fault-bounded half-grabens (Oliveira et al., 1991), is revealed by the development of Cambrian-Series-2 shelly carbonate production punctuated with microbial-archaeocyathan reefal complexes (Moreno-Eiris, 1987). This rifting activity is also demonstrated by the presence of felsic and mafic volcanic rocks within the Cambrian sedimentary sequence. The volcanic rocks are initially characterized as calc-alkaline and peraluminous, referred to as the "Early Rift Event" (Sánchez-García et al., 2010, 2019), but subsequently transitioned into bimodal magmatism, known as the "Main Rift Event" (Mata and Munha, 1990; Sánchez-García et al., 2010, 2019). During the late Cambrian to early Ordovician, this magmatism exhibits an alkaline to peralkaline character (Carrilho Lopes, 2004; Díez-Fernández et al., 2014), referred to as the "Late Rift Event" (Sánchez-García et al., 2019).

The transition from the final stages of the Cadomian Orogeny in the Neoproterozoic to the beginning of the Variscan Cycle in the Cambrian is notably recorded along the southern margin of the OMZ, namely in the EAMB. The EAMB comprises medium-to-high-grade Variscan metamorphic units, locally juxtaposed by low-grade Devonian-to-Carboniferous basins (e.g.: Pereira et al., 2009). These medium-to-high-grade units consist of Ediacaran metasediments overlain by Lower Palaeozoic volcano-sedimentary and detrital-carbonate sequences (Fig. 1b). The Ediacaran metasediments consist of black paragneisses and metacherts of the Série Negra Group in the Évora Massif (Carvalhosa and Zbyszewski, 1994; Chichorro et al., 2008; Pereira et al., 2003), and the La Umbría formations (Séries de "la Umbria") in the Aracena Metamorphic Belt (Díaz-Azpiroz et al., 2004 and references therein). Meanwhile, the bottom section of the Lower Palaeozoic sequences is predominantly composed of felsic rocks, namely rhyolites and rhyodacites, which were metamorphosed into felsic schists and orthogneisses during the Variscan orogeny (Fig. 1c and d). This domain, characterized by the predominance of felsic mylonites, is always associated with siliciclastic and carbonate metasediments. Notwithstanding the mylonitic deformation, it is feasible to delineate, in certain areas, metabasites interspersed and boudinated within the marbles or intersecting the calc-silicate layering (Chichorro et al., 2008). The volcano (essentially felsic)-sedimentary and carbonate complexes are prominently represented in the Monfurado Formation (Carvalhosa and Zbyszewski, 1994; Chichorro et al., 2008) in Évora, as well as in the Jabugo formation in Aracena (Bard, 1969). This domain transitions upwards to well-defined

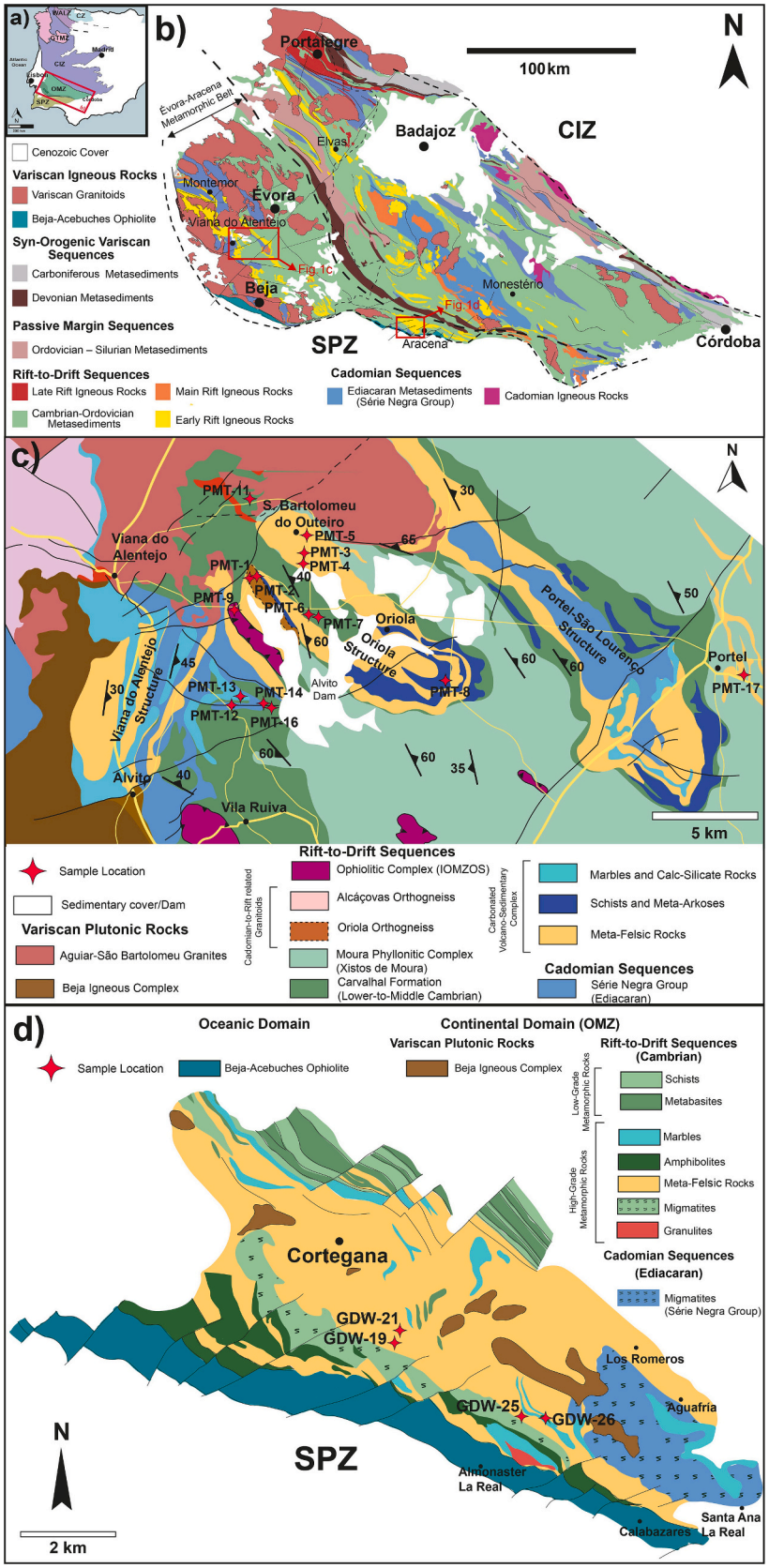

Fig. 1. – Geological setting of the studied area represented by a red rectangle, within: a) the Iberian Massif (adapted from Moreira, 2017); b) the Ossa-Morena Zone; c) geological map of the Viana do Alentejo region with the location of all collected samples in this region (adapted from Ferreira and Piçarra, 2020); and d) geological map of the Aracena Massif with the location of all collected samples in this region (adapted from Díaz-Azpiroz et al., 2006). (For interpretation of the references to colour in this figure legend, the reader is referred to the web version of this article.)

and elongated bands parallel to the orogen, where the mafic igneous rocks (greenschists or amphibolites) predominate in relation to felsic rocks. This domain is well evidenced by the Carvalhal and Xistos de Moura formations (Carvalhosa and Zbyszewski, 1994), on the Portuguese side, and in the La Corte Formation (Bard, 1969; Giese et al., 1994), in Spain.

The whole EAMB is significantly dismembered by the Variscan Orogeny. The development of medium to high-grade metamorphic rocks is linked to the intra-orogenic extensional event D2-D3, which has been interpreted as compatible with an oblique extensional scenario, contemporaneous with a Visean thermal event in the OMZ (Díaz-Azpiroz et al., 2006; Pereira et al., 2009). Within the Évora Massif, high-grade rocks (upper amphibolite to granulite facies) are retained in metamorphic core-complexes surrounded by lower-to-middle-grade rocks. North of the high-grade metamorphic core in the Évora region, medium-grade rocks (amphibolite facies) are predominant, whereas to the south, along the Montemor-o-Novo shear, low- to medium-grade rocks (greenschist to amphibolite facies) are present. The contact between these domains occurs via transcurrent and transtensive shear zones (Pereira et al., 2009), which fundamentally delineate the high-grade cores (footwall sections) from a medium-low-grade hanging wall. In the Aracena Massif, an extensional shear zone of the Variscan D2 phase (Díaz-Azpiroz et al., 2006) separates a high-grade domain to the south from a medium- and low-grade domain to the north.

3. Methods

Twenty-two samples were collected in the EAMB, distributed over two regions: Viana do Alentejo and Aracena Massif (Fig. 1c and d; Table 1). The Viana do Alentejo region is geographically divided in 4 sectors: São Bartolomeu do Outeiro, Oriola, Viana Dam and Portel-São Lourenço.

All samples were prepared for petrographic analysis at LNEG – Laboratório Nacional de Energia e Geologia and in DG-FCUL – Departamento de Geologia da Faculdade de Ciências da Universidade de Lisboa. All minerals mentioned in the Petrography section were confirmed by EPMA at DG-FCUL – Departamento de Geologia da Faculdade de Ciências da Universidade de Lisboa. This data is not relevant for this work, reason why it is not presented, but it can be provided if requested to the authors.

3.1. Whole rock geochemistry

The meta-volcanic samples (both mafic and felsic) were also the subject of whole-rock elemental geochemical analyses performed at Activation Laboratories (Ontario, Canada), using standardized

Table 1
Summary table of the samples covered in this work.

Rock Type	Region	Sector	Sample	Coordinates	Petrography	Whole Rock Geochemistry	Sr-Nd Isotopes	Geochronology
Meta-Felsic Rocks	Viana do Alentejo Region	Oriola	PMT-1	38°20′02”N 7°55′41”W	x	x	x	
			PMT-2	38°20′02”N 7°55′39”W	x	x	x	x
		São Bartolomeu do Outeiro	PMT-3	38°20′31”N 7°54′17”W	x	x	x	
			PMT-5	38°21′07”N 7°54′10”W	x	x	x	
		Viana Dam	PMT-12A	38°17′15”N 7°56′23”W	x	x	x	
		Portel-São Lourenço	PMT-17	38°18′01”N 7°42′15”W	x	x		x
	Aracena Massif		GDW-19	37°53′46”N 6°48′17”W	x	x	x	
			GDW-21	37°53′43”N 6°48′24”W	x	x	x	x
			GDW-25	37°53′01”N 6°46′52”W	x	x	x	x
Metamafic Rocks	Viana do Alentejo Region	Oriola	PMT-9A	38°19′25”N 7°56′18”W	x	x	x	
			PMT-9B	38°19′25”N 7°56′18”W	x	x	x	
			PMT-9C	38°19′25”N 7°56′18”W	x	x	x	
			PMT-6	38°19′17”N 7°54′06”W	x	x	x	
			PMT-8C	38°17′49”N 7°50′10”W	x	x	x	
			PMT-7	38°19′17”N 7°53′57”W	x	x	x	
		São Bartolomeu do Outeiro	PMT-11A	38°21′51”N 7°55′49”W	x	x	x	
			PMT-4	38°20′30”N 7°54′17”W	x	x	x	
		Viana Dam	PMT-12B	38°17′15”N 7°56′23”W	x	x	x	x
			PMT-13	38°17′27”N 7°56′07”W	x	x	x	
			PMT-14	38°17′19”N 7°55′28”W	x	x	x	
			PMT-16	38°17′08”N 7°55′14”W	x	x	x	x
	Aracena Massif		GDW-26	37°52′43”N 6°46′26”W	x	x	x	

procedures for ICP-OES analysis (Inductively Coupled Plasma Optical Emission Spectrometry) of major elements and ICP-MS for trace elements. Samples were mixed with lithium metaborate and lithium tetraborate and fused in an induction furnace. The obtained molten melt was added into 5 % nitric acidic a solution containing an internal standard, which was mixed continuously until complete dissolution. Samples were subsequently diluted for ICP-MS analysis. Such analyses occurred in batch systems where each batch contained a method blank, certified reference materials (DNC-1, GBW 07113, SY-4, BIR-1a, BCR-2, W-2b) and 6 % replicates. 14 prepared USGS and CANMET certified reference materials were used for calibration. Three blanks and five controls (three before the samples sample and two after) were analysed on each group of samples. Duplicates were fused and analysed every fifteen samples. To ensure the accuracy of the results, one of the fourteen standards was utilized during the analysis for each group of 10 samples, and the device was recalibrated after forty samples.

3.2. Isotope geochemistry

Rb—Sr and Sm—Nd isotopic compositions were determined using a Triton + Thermo-Scientific mass spectrometer in the Laboratory of Géosciences Environnement Toulouse - Observatoire Midi-Pyrénées (GET-OMP) in Toulouse, France, following procedures described by Li et al. (2012). The procedure for each sample consisted of dissolving about 100 mg of total rock powder with a 1:1 HF/HNO_3 mixture. Subsequently, all samples were diluted in 5 ml of 2 % HNO_3, with part of the solution being removed for analysis in the ICP-MS Element XR, to obtain the precise $^{87}Rb/^{86}Sr$ and $^{147}Sm/^{144}Nd$ ratios. The remainder was dried, and Nd/Sr was extracted from the matrix using a combination of Sr-Spec and Thru-spec Eichrom resins. The mixture of Sr and REE was subsequently loaded onto a Re filament, run sequentially (first Sr and then Nd), using a double filament protocol in Re. The monitoring of ^{87}Rb and ^{144}Sm interferences was performed according to Li et al. (2012). The quality and reproducibility of the measurements were controlled using a sequential measurement of the isotopic standards (NBS 987 and La Jolla), doped isotopic standards (NBS 987+ Rb and La Jolla + Sm) and artificial Sr + REE. The reproducibility of the standards was 0.510845 +/− 6 ($n = 13$) for La Jolla and 0.710279 +/− 8 ($n = 15$) for NBS-987 (pure and doped), being within the recommended values. The measured blanks were 54 pg for Nd and 58 pg for the isotopic ratios of Sr. $^{87}Sr/^{86}Sr$ and $^{143}Nd/^{144}Nd$ were normalized against $^{86}Sr/^{88}Sr = 0.1449$ and $^{146}Nd/^{144}Nd = 0.7219$, respectively, after correcting isobaric interferences using $^{87}Rb/^{85}Sr = 0.387041$ at ^{87}Sr and a combination of $^{147}Sm/^{149}Sm = 1.08583$ and $^{147}Sm/^{144}Sm = 4.87090$ at ^{144}Nd. The values of the $^{145}Nd/^{144}Nd$ ratios are given to illustrate the precise corrections of Sm isobaric interferences.

The εNd_i and $^{87}Sr/^{86}Sr_i$ values were recalculated following the procedures established in Bento dos Santos et al. (2011) for 320 Ma, since this is the minimum age typically attributed to the final high-temperature Variscan metamorphic/metasomatic event, associated with the final intra-orogenic episode of the Variscan collision, that affected the studied region (Gomes and Fonseca, 2006). Recalculation for other significant ages, namely 500 Ma, were performed and no significant variation was found in εNd_i and $^{87}Sr/^{86}Sr_i$ (e.g.: εNd_i changes are smaller than +1, except where Rb/Sr and Sm/Nd ratios are abnormally high or low compared to the typical crustal values). The value of 6.54×10^{-12} a^{-1} was used for the ^{147}Sm decay constant after Lugmair and Marti (1978). Further, it considers the $^{143}Nd/^{144}Nd$ and $^{147}Sm/^{144}Nd$ ratios of 0.512638 and 0.1967, respectively, according to DePaolo and Wasserburg (1979) for the Chondritic Uniform Reservoir (CHUR) to calculate εNd. For the calculation of model ages (T_{DM2}), the procedures established in Bento dos Santos et al. (2011) and the equations of Liew and Hofmann (1988) were used with 320 Ma being the intermediate stage.

3.3. LA-ICP-MS zircon geochronology

Regarding geochronological data, zircon concentrates were separated from 1 to 2 kg sample material at the DG-FCUL – Departamento de Geologia da Faculdade de Ciências da Universidade de Lisboa. This material was crushed using a jaw crusher and then sieved for the fraction below 250 μm. Heavy mineral separation was carried out by using a Wilfley table and final selection of the zircon grains for U—Pb dating was achieved by hand-picking under a binocular microscope. Cathodoluminescence (CL)-imaging was also performed prior to U—Pb analysis at HERCULES Laboratory, in Évora. Zircons were analysed at Laboratório de Geocronologia da Universidade de Brasília and at the Senckenberg Naturhistorische Sammlungen, Dresden.

At Laboratório de Geocronologia da Universidade de Brasília analyses were performed by LA-ICP-MS using a Thermo Finnigan Neptune Multicoletor ICP-MS coupled to New Wave UP213 Nd: YAG (213 nm) laser, following the procedures described by Bühn et al. (2009). GJ1 and 91,500 (Jackson et al., 2004) standards were analysed together with the studied samples. The carrier gas employed was Helium (He), which was combined with Argon (Ar) before to integration into the ICP-MS. The laser was operated at a frequency of 10 cycles per second (Hz), and throughout the ablation process, 40 cycles of 1.049 s each were used to take isotopic mass measurements. The laser has a spot size of 25 μm, with a fluence between 3.0 and 3.5 J/cm^2. Afterwards, only the coherent response periods of the signal during the ablation were deemed legitimate in the analysis of the acquired data. This mass spectrometer is fitted with a multi-collector which is linked to six distinct masses: ^{238}U, ^{235}U, ^{207}Pb, ^{206}Pb, $^{204}Hg/^{204}Pb$, and ^{202}Hg. The isotopes ^{238}U and ^{206}Pb are examined using Faraday cups, while ^{207}Pb and ^{202}Hg are detected and monitored using ion counters. The inclusion of the ^{204}Pb isotopes was determined by calculating the natural ratio of $^{202}Hg/^{204}Hg$ to be 4.346. As the spectrometer cannot distinguish between the presence of mercury and/or lead, this signal is quantified using the ratio $^{204}Hg/^{204}Pb$. Concurrently, the ^{202}Hg is being acquired to incorporate a correction for helium interference. As it is filtered via a sieve to eliminate the influence of ^{204}Hg before being injected into the vacuum, it always contains traces of mercury. Using an Excel spreadsheet created by technicians from Geocron-IG/UnB, the data reduction was performed, considering blank values, zircon pattern composition, and error propagation. A typical Pb correction is implemented on zircons with a $^{206}Pb/^{204}Pb$ ratio below 1000, utilizing a standard lead composition derived from the Stacey and Kramers (1975).

Meanwhile, at the Senckenberg Naturhistorische Sammlungen, in Dresden, analyses were performed by LA-SF ICP-MS using a Thermo-Scientific Element 2 XR sector field ICP-MS (single-collector) coupled to a RESOlution 193 nm excimer laser. Each analysis consisted of 15 s background acquisition followed by 30 s data acquisition, using a laser spot-size of 15, 25 and 35 μm. A common-Pb correction was carried out, if necessary, based on the interference- and background-corrected ^{204}Pb signal and a model Pb composition (Stacey and Kramers, 1975). The necessity of the correction is judged on whether the corrected $^{207}Pb/^{206}Pb$ lies outside of the internal errors of the measured ratios (Frei and Gerdes, 2009). Raw data were corrected for background signal, common Pb, laser-induced elemental fractionation, instrumental mass discrimination, and time-dependant elemental fractionation of Pb/Th and Pb/U using an Excel spreadsheet program developed by Axel Gerdes (Institute of Geosciences, Johann Wolfgang Goethe University Frankfurt, Frankfurt am Main, Germany). Reported uncertainties were propagated by quadratic addition of the external reproducibility obtained from the standard zircon GJ-1 (~0.6 % and 0.5–1 % for the $^{207}Pb/^{206}Pb$ and $^{206}Pb/^{238}U$, respectively; Jackson et al., 2004) during individual analytical sessions and within-run precision of each analysis. In order to test the accuracy of the measurements and data reduction, we included the Plešovice zircon as a secondary standard in our analyses, which gave reproducibly ages of c. 337 Ma, fitting with the results of Sláma et al. (2008).

Concordia diagrams (2r error ellipses), Concordia ages (95 % confidence level) and relative probability plots were produced using IsoplotR (Vermeesch, 2018). Geological interpretations are based solely on concordant analyses with concordance comprised between 90 % and 110 %. These were calculated between $^{206}Pb/^{238}U$ and $^{207}Pb/^{235}U$ for zircons with age < 1000 Ma, and between $^{206}Pb/^{238}U$ and $^{207}Pb/^{235}U$ for zircons with age > 1000 Ma, following the procedures referred in Ferreira et al. (2022).

4. Petrography

4.1. Meta-felsic rocks

A total of nine meta-felsic samples were collected, six in the Viana do Alentejo region (one from Portel-São Lourenço sector, two from Oriola sector, two from São Bartolomeu do Outeiro sector, one from Viana Dam sector) and three from the Aracena Massif.

The meta-felsic rocks of the Viana do Alentejo region present a grano-lepidoblastic to granoblastic texture, with hand specimens being very light coloured (Fig. 2a). Quartz is the most abundant mineral phase by far, although the rocks from the Oriola sector show a large abundance of phyllosilicates (mainly muscovite), which tend to occur in a preferential direction, defining a planar anisotropy concordant with the regional deformation (Fig. 2b and 3a). Such abundance of mica and orientation is also evident in hand specimen. Most meta-felsic rocks of the Viana do Alentejo region also present feldspar (typically plagioclase) and accessory mineral phases like rutile, zircon, and oxides, as well as late chlorite veins in one sample (PMT-12 A; Fig. 3b).

As for the meta-felsic samples from the Aracena Massif, these have a granoblastic texture and occasionally presents a preferential orientation (Fig. 2c), which is consistent with their overall lithology (being orthogneisses). These meta-felsic rocks are mainly composed of alkali feldspar, quartz, and biotite, with the latter being occasionally chloritized. Some plagioclase, muscovite and oxides are also observed.

4.2. Meta-mafic rocks

Thirteen meta-mafic rocks were sampled for this study: twelve from the Viana do Alentejo region (six from the Oriola sector, two from São Bartolomeu do Outeiro sector, four from Viana Dam sector) and one from the Aracena Massif. The meta-mafic rocks show dark, slightly bluish colours, occasionally presenting oriented dark or green minerals (amphibole and/or epidote; Fig. 2d).

Two petrographic types can be recognized: a) coarse-to-medium grained banded amphibolites b) mafic schists.

Mafic schists/greenschists present an essentially nematoblastic texture (Fig. 3c), being mainly composed of amphibole, occasionally retrogressed to chlorite, and feldspar. Greenschists also have frequent crystals of epidote (Fig. 3d) and, occasionally, titanite and oxides.

Amphibolites are mostly composed of amphibole, while also

Fig. 2. – Field observations: a) general overview of the meta-felsic PMT-2 outcrop; b) detailed view of PMT-2 outcrop; c) detailed view of orthogneiss GDW-21 hand specimen; and d) detailed view of meta-mafic PMT-6 hand specimen.

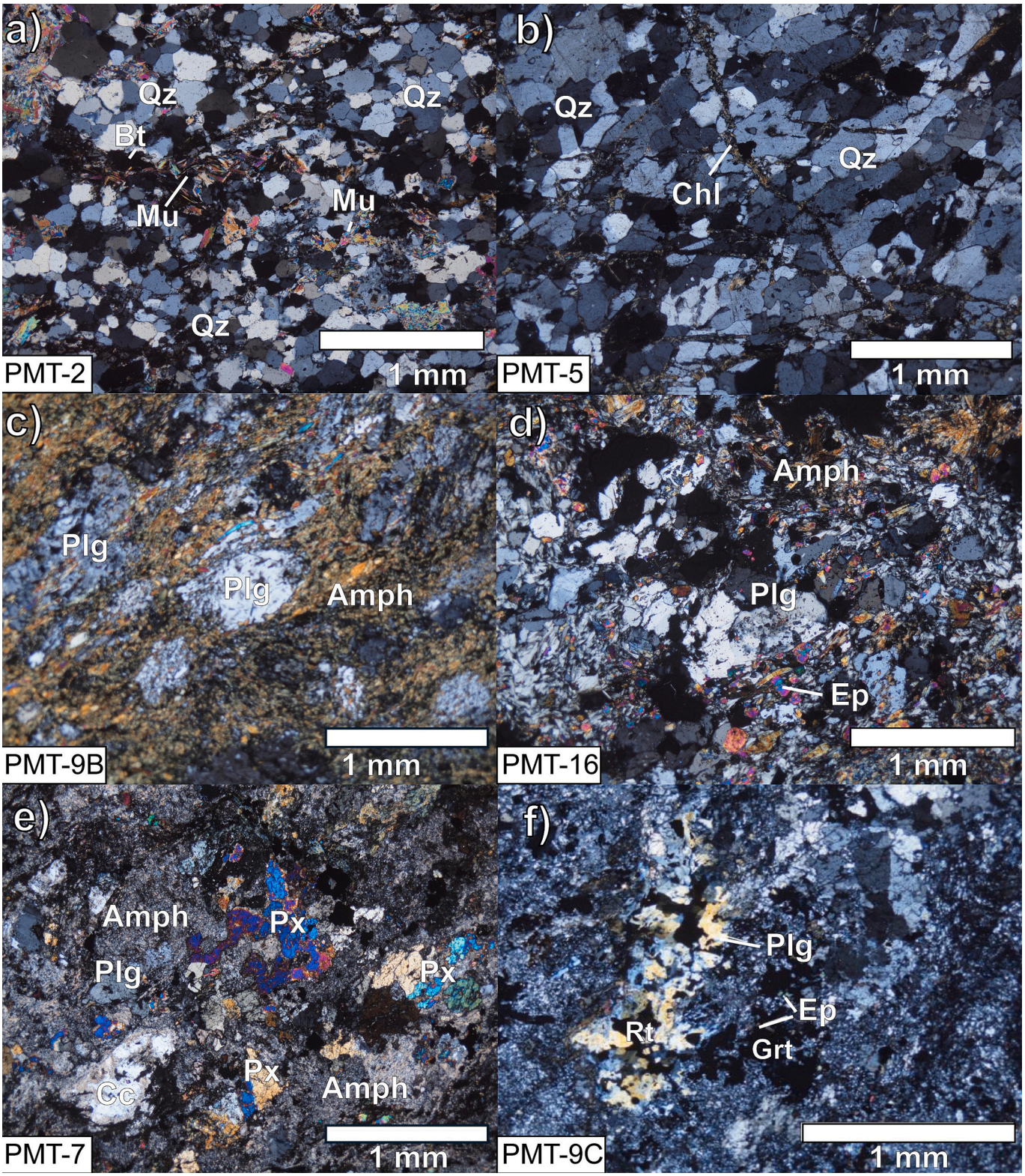

Fig. 3. – Micropetrographic features of the meta-volcanic rocks from the Viana do Alentejo region: a) thin muscovite and biotite surrounding the predominant quartz portions in a meta-felsic sample of PMT-2; b) abundant quartz and frequent feldspar in meta-felsic sample PMT-5; c) anastomosed (deformed) texture with amphibole surrounding feldspar crystals in one of the greenschist-facies samples (PMT-9B); d) frequent epidote in meta-mafic sample PMT-16; e) abundant pyroxene in amphibolites (PMT-7); and f) garnet associated with epidote in meta-mafic sample PMT—9C.

presenting Ca-rich pyroxene (Fig. 3e) and sporadic calcite, exhibiting nematoblastic to granoblastic textures. Some samples also have garnet, which occasionally occur in association with epidote (Fig. 3f).

5. Whole rock geochemistry

The whole-rock geochemical results from twenty-two samples from the EAMB (nine meta-felsic and thirteen meta-mafic) are presented in

Table 2
Whole-rock geochemical data of the studied rocks from the Évora-Aracena Metamorphic Belt, SW OMZ.

Rock Type	Meta-Felsic Rocks								
Sector	Oriola		São Bartolomeu do Outeiro		Viana Dam	Portel-São Lourenço	Aracena Massif		
Sample	PMT-1	PMT-2	PMT-3	PMT-5	PMT-12A	PMT-17	GDW-19	GDW-21	GDW-25
SiO_2	88.19	87.83	77.27	79	71.7	64.5	76.29	74.2	72.45
TiO_2	0.45	0.46	0.3	0.15	0.28	0.17	0.116	0.586	0.708
Al_2O_3	6.73	6.86	13.03	11.9	14.5	17.9	12.7	10.91	16.28
Fe_2O_3	1.28	1.08	1.14	0.6	3.5	4.59	0.91	3.33	1.37
MnO	0.01	0.01	0.01	0.01	0.04	0.04	0.016	0.029	0.056
MgO	0.17	0.17	0.14	0.03	0.63	0.03	0.11	0.6	0.04
CaO	0.05	0.16	0.25	0.43	0.76	0.04	0.36	0.47	1.29
K_2O	1.86	2.09	0.2	0.84	0.24	5.49	2.4	6.17	0.85
Na_2O	0.31	0.86	5.9	5.55	7.59	7.06	5.24	1.2	6.96
P_2O_5	< 0.01	0.05	< 0.01	< 0.01	0.03	0.03	< 0.01	0.05	0.03
LOI	1.41	0.98	2.06	0.45	0.87	0.55	0.81	0.47	0.67
Total	99.05	99.57	98.23	98.51	99.27	99.85	98.94	98.02	100.7
Sc	4	4	8	3	8	1	5	8	15
V	25	25	12	2.5	33	2.5	< 5	45	24
Cr	20	20	10	10	10	5	< 20	40	< 20
Co	56	53	151	37	40	2	126	94	72
Ni	10	10	10	10	10	0.5	< 20	< 20	< 20
Ga	8	8	19	23	17	34.2	22	15	26
Ge	1	1	0.5	1	0.5	2.5	2	2	2
Rb	50	59	7	15	4	124.5	42	164	16
Sr	12	32	40	34	35	34.1	22	49	70
Y	21	21	57	49	59	73.2	7	21	71
Zr	529	511	260	293	286	1800	140	185	171
Nb	7	8	5	7	3	277	3	13	10
Ag	2.2	2.2	1.1	1.1	1.2	0.25	< 0.5	< 0.5	< 0.5
Sn	1	1	2	5	1	8	2	4	4
Ba	369	360	21	187	119	165	202	839	147
Hf	12.7	12.2	6.4	9.6	7.4	38.3	5	4.5	4.9
Ta	0.9	0.9	0.6	0.8	0.3	17.5	0.2	1.8	0.8
W	550	532	799	375	352	3	1040	871	609
Th	20.8	21	9.5	10.4	3.5	24.2	3.1	5.6	10.2
U	3	3	2.5	4.3	1	7.68	0.9	2	1.4
La	22.7	31.4	44.5	23.9	10.2	66.1	21.3	25.3	70.4
Ce	54.8	72.8	94	33.5	25.4	150	46.7	46.6	91.2
Pr	5.46	7.08	11	5.65	3.36	15.25	5.69	6.11	18.9
Nd	21	27.1	44.4	22.5	15.3	49.1	21.2	23.5	71.1
Sm	4.1	5.1	10.4	4.9	4.4	9.46	3.8	4.6	16
Eu	0.72	0.88	1.59	0.64	0.76	0.45	0.49	0.71	1.59
Gd	3.6	4.2	9.6	5.7	5.7	7.86	2.4	3.9	13.6
Tb	0.5	0.6	1.6	1	1.2	1.76	0.3	0.6	2.3
Dy	3.2	3.4	9.7	7.5	8.7	12.7	1.4	3.8	13.9
Ho	0.7	0.7	2	1.8	2	2.88	0.2	0.8	2.7
Er	2	2	5.9	5.8	6.3	9.15	0.8	2.2	7.3
Tm	0.29	0.31	0.93	0.92	0.95	1.49	0.1	0.32	1.08
Yb	2.1	2	6.1	6.3	6.9	9.85	0.8	2.2	6.8
Lu	0.36	0.34	0.93	0.99	1.04	1.64	0.14	0.37	1.01
Pb	2.5	5	2.5	2.5	2.5	1	< 5	< 5	< 5
Cs	0.7	0.25	0.25	0.25	0.25	0.43	< 0.5	9.1	< 0.5

Rock Type	Metamafic												
Sector	Oriola						São Bartolomeu do Outeiro		Viana Dam				Aracena Massif
Sample	PMT-9A	PMT-9B	PMT-9C	PMT-8C	PMT-6	PMT-7	PMT-11A	PMT-4	PMT-12B	PMT-13	PMT-14	PMT-16	GDW-26
SiO_2	48.47	50.92	47.24	42.83	47.62	49.66	49.34	48.31	51.85	42.1	51.03	44.59	47.39
TiO_2	1.4	0.97	0.89	3.55	1.67	1.93	1.77	0.96	2.3	2.06	1.87	0.67	3.376
Al_2O_3	16.08	15.13	17.36	15.26	15.43	14.66	14.5	14.98	14.04	15.55	14.2	20.12	13.25
Fe_2O_3	9.64	9.43	9.79	13.97	11.28	10.91	12.62	8.68	12.31	13.44	10.65	7.44	14.7
MnO	0.18	0.18	0.19	0.17	0.2	0.22	0.24	0.19	0.35	0.2	0.18	0.12	0.144
MgO	7.28	7.24	4.67	8.25	3.96	4.07	7.04	4.14	5.25	4.29	6.19	8.64	4.52
CaO	10.84	10.9	13.44	9.35	14.49	11	10.32	17.8	6.57	19.75	9.97	10.66	10.46
K_2O	0.42	0.25	2.16	0.05	0.47	1.08	0.39	0.59	0.93	0.07	0.35	0.22	0.68
Na_2O	3.63	3.78	2.13	2.79	2.97	3.75	3.18	2.51	4.17	0.37	3.61	3.05	4.34
P_2O_5	0.16	0.09	0.05	0.51	0.19	0.26	0.17	0.07	0.21	0.23	0.28	0.04	0.45
LOI	1.09	1.11	2.67	3.67	1.99	1.41	1.01	2.4	1.34	2.42	1.41	4.83	0.92
Total	98.1	98.9	97.92	96.73	98.28	97.54	99.57	98.23	97.98	98.06	98.34	95.54	100.2
Sc	33	26	32	22	38	38	47	33	40	38	42	25	46
V	230	173	158	301	239	256	365	163	384	301	316	158	461
Cr	290	320	840	290	190	50	240	400	20	80	50	350	< 20

(*continued on next page*)

Table 2 (*continued*)

Rock Type	Metamafic												
Sector	Oriola						São Bartolomeu do Outeiro		Viana Dam				Aracena Massif
Sample	PMT-9A	PMT-9B	PMT-9C	PMT-8C	PMT-6	PMT-7	PMT-11A	PMT-4	PMT-12B	PMT-13	PMT-14	PMT-16	GDW-26
Co	47	55	53	53	55	51	52	54	36	42	44	49	54
Ni	130	140	240	180	100	60	90	190	30	80	70	200	20
Ga	15	13	14	21	18	17	17	11	21	25	20	13	26
Ge	1	1	1	2	2	2	2	2	2	2	2	0.5	2
Rb	5	3	65	1	15	41	15	18	34	1	8	6	8
Sr	246	242	351	1457	440	377	264	941	143	873	303	114	167
Y	20	14	17	25	24	28	31	17	34	27	24	13	56
Zr	96	65	43	213	125	147	109	64	103	142	131	32	169
Nb	6	3	2	49	8	12	4	0.5	2	10	12	0.5	7
Ag	0.25	0.25	0.25	0.7	0.5	0.6	0.25	0.25	0.25	0.5	0.5	0.25	< 0.5
Sn	1	1	1	2	1	1	1	1	2	1	1	< 1	2
Ba	150	68	487	37	127	203	25	224	256	15	119	57	139
Hf	2.5	1.7	1.3	5.2	3.1	3.6	2.8	1.7	3.3	3.8	3.2	0.8	4.8
Ta	0.5	0.3	0.2	3.2	0.7	0.9	0.3	0.05	0.2	0.8	0.9	0.05	0.4
W	76	101	116	40	130	78	79	92	144	134	98	49	148
Th	0.5	0.3	0.2	4.2	0.7	1.2	0.3	0.2	1.3	0.8	0.9	0.05	1.9
U	0.2	0.1	0.05	1.1	0.2	0.3	0.2	0.1	0.7	0.3	0.4	0.05	1.5
La	7.2	4.1	2.8	37.6	8.4	13.4	5.6	2.3	5.5	11.4	16.7	0.9	15.9
Ce	17.5	10.5	6.7	75.5	21.3	30.9	14.9	7.2	13.9	28.2	37.8	3.3	38.6
Pr	2.36	1.51	0.99	9.06	2.88	4.11	2.28	1.15	2.08	3.77	4.86	0.62	5.43
Nd	11.6	7.9	5.6	38.1	13.9	18.8	12.1	6.4	10.9	18.1	22.2	3.7	25.8
Sm	3.2	2.4	1.9	7.8	3.9	4.9	4	2.2	3.8	5.2	5.4	1.4	7.6
Eu	1.31	1.07	0.74	2.71	1.42	1.78	1.43	0.9	1.65	1.82	2.22	0.62	2.24
Gd	3.7	2.9	2.7	7.5	4.6	5.5	5.2	2.9	5.5	5.7	5.6	2	8.1
Tb	0.6	0.5	0.5	1	0.8	0.9	0.9	0.5	0.9	1	0.8	0.3	1.5
Dy	3.8	3.1	3.1	5.4	4.7	5.5	6	3.2	6.4	5.6	4.9	2.3	9.8
Ho	0.8	0.6	0.7	1	1	1.1	1.2	0.7	1.4	1.1	1	0.5	2
Er	2.1	1.8	1.9	2.6	2.7	3.1	3.6	2	4.1	3.2	2.6	1.4	5.7
Tm	0.29	0.24	0.28	0.34	0.38	0.43	0.54	0.29	0.59	0.45	0.37	0.2	0.81
Yb	2	1.5	1.8	2	2.6	2.9	3.4	1.8	3.9	2.9	2.4	1.3	5.2
Lu	0.3	0.25	0.27	0.29	0.38	0.43	0.53	0.28	0.63	0.46	0.35	0.2	0.8
Pb	8	6	26	20	12	7	7	34	2.5	5	6	5	7
Cs	0.25	0.25	2.3	0.25	0.7	1	0.5	0.6	1.3	0.25	0.7	0.25	0.7
K/P	4.99	5.28	82.18	0.19	4.71	7.9	4.36	16.03	8.42	0.58	2.38	10.46	2.8742363
Ti/Yb	4280.55	3932.11	3020.43	10,988.29	3920.43	4088.38	3139.67	3268.29	3609.77	4340.46	4752.61	3228.92	3892.1154

K/P and Ti/Yb only calculated for metamafic rocks. Major elements in Wt%. trace elements in ppm.

Table 2.

Meta-felsic rocks mostly classify as rhyolites, whereas meta-mafic rocks plot into the basalts field in the Jensen (1976) classification diagram (Appendix 1a). In the Nb/Y vs. Zr/TiO_2 classification diagram (Winchester and Floyd, 1977; Appendix 1b) meta-felsic rocks plot in the rhyolite and rhyodacite/dacite fields, except for the Portel-São Lourenço, sample which corresponds to a phonolite (PMT-17), and a sample from Aracena Massif that plots in the andesite field. As for meta-mafic rocks, these classify mainly as subalkaline basalts or andesites/basalts, with only sample PMT-8C plotting in the alkaline basalts field. These diagrams are more adequate since they use strongly immobile elements in low-to-medium-grade metamorphic conditions. The meta-felsic samples constitute a calc-alkaline sequence (Appendix 1c), showing a progressive increase in iron, while also presenting a weak to strong peraluminous character (Appendix 1d). The meta-mafic rocks show a strong metaluminous character (A/NK > 1.8; Appendix 1d) and a transitional (tholeiitic to calc-alkaline) nature (Appendix 1c).

In Harker-type diagrams using SiO_2 as a fractionation index (Appendix 2), the meta-felsic rocks display positive correlations for TiO_2 and K_2O, while Al_2O_3, Na_2O and FeOt present negative correlations. It should be noted that for K_2O and Na_2O a slight dispersion is observed. Concerning CaO, MgO and P_2O_5, there are no significant variations in their concentrations. The meta-mafic samples present a positive correlation for TiO_2, K_2O, Na_2O, P_2O_5 and FeOt and negative correlations for CaO, Al_2O_3 and MgO. However, for MgO, P_2O_5 and FeOt a significant dispersion is evident.

In the Rare Earth Elements (REE) patterns, meta-felsic rocks are always enriched in LREE (Fig. 4a), presenting values of $(La/Lu)_N$ between 1.05 and 15.8, and the presence of a negative Eu anomaly in all samples ($Eu/Eu^* = 0.32–0.56$; Fig. 4a). In this diagram, the sample GDW-19 from the Aracena Massif presents the lowest HREE contents (HREEt = 6.14 ppm; Fig. 4a). Oriola's meta-felsic rocks and sample GDW-21 from Aracena are slightly more enriched in these same elements (HREEt = 9.15–9.35 ppm; Fig. 4a), while the rocks from São Bartolomeu do Outeiro, Viana Dam, and Portel-São Lourenço sectors and sample GDW-25 from the Aracena Massif are the most enriched in HREE (HREEt = 24.31–39.47 ppm; Fig. 4a). However, samples GDW-25 from the Aracena Massif and PMT-17 from the Portel-São Lourenço sector exhibit high contents of both LREE and HREE, indicating a more significant enrichment in total REE content compared to the São Bartolomeu do Outeiro and Viana Dam samples (REEt = 317.88 and 337.69 ppm, respectively; Fig. 4a). In turn, the mafic rocks present very variable $(La/Lu)_N$ ratios (0.47–13.46; Fig. 4b). Consequently, the REE diagram for these rocks displays a fan-like pattern for the LREE, whereas for the HREE, these rocks have a more flattened and constant pattern (Fig. 4b).

The incompatible elements normalized diagrams for the meta-felsic rocks show a significant correlation with the upper crust, as evidenced by the abundance of the typically more immobile elements (e.g.:, Th, U, La, Ce, Nd, Hf, Zr, Sm, Tb, Y, Tm and Yb; Fig. 4c). In turn, the meta-mafic rocks display positive anomalies in Pb and Sr and minor negative anomalies of P and Nb, and a significant correlation with *E*-MORB (Fig. 4d), particularly in the high-field strength elements (HFSE), such as Nd, Zr, Sm, Y, Yb and Lu.

In the Pearce et al. (1984); Fig. 5a and b) tectonic discrimination

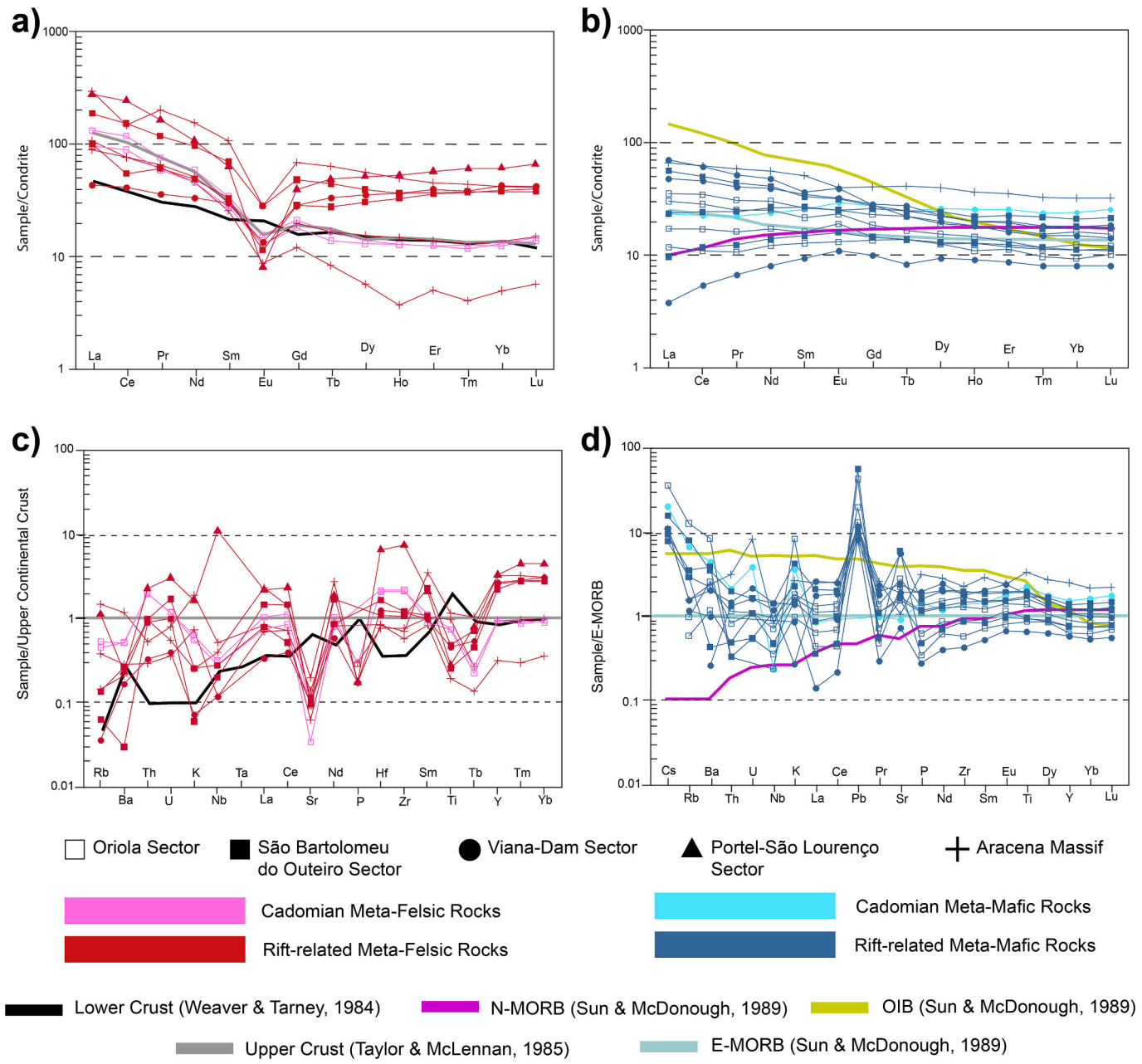

Fig. 4. – a) Chondrite-normalized (McDonough and Sun, 1995) REE patterns for the meta-felsic rock samples; b) Chondrite-normalized (McDonough and Sun, 1995) REE patterns for the meta-mafic rock samples; c) Multi-elemental diagram for the meta-felsic rock samples, normalized to the upper continental crust (Taylor and McLennan, 1995); d) Multi-elemental diagram for the meta-mafic samples, normalized to *E*-MORB (McDonough and Sun, 1995).

diagrams, it is possible to distinguish, again, three groups of meta-felsic samples, although not exactly the same as in the REE diagrams. The meta-felsic rocks from São Bartolomeu do Outeiro and Viana Dam sectors and sample GDW-25 from Aracena Massif plot in the ocean ridge granites (ORG) field, while Oriola's meta-felsic rocks and samples GDW-19 and GDW-21 from Aracena display a volcanic arc granite (VAG) signature. As for the Portel-São Lourenço meta-rhyolite, it presents an intraplate granite (WPG) signature.

The meta-mafic rocks show an E-MORB/N-MORB transition in the Wood (1980) Th-Hf/3-Nb/16 diagram (Fig. 5c), except for sample PMT—8C, that has an alkaline intraplate basalt signature (Within Plate Alkaline Basalts - WPA); and sample PMT—12B, characterized by a continental crust signature (Calc-Alkaline Basalts - CAB) and positioned outside the MORB-OIB array in the Pearce (2008) tectonic diagram (Fig. 5d), similar to the amphibolite from the Aracena Massif (GDW-26).

6. Isotope geochemistry

Rb—Sr and Sm—Nd data obtained from the studied meta-volcanic rocks and initial epsilon values and T_{DM2} model ages are listed in Table 3 and plotted in Fig. 6.

The isotopic data of the sampled meta-felsic rocks also show the presence of three distinct groups. São Bartolomeu do Outeiro and Viana Dam meta-felsic rocks have εNd_{320} values between −0.7 and + 3.0 with $^{87}Sr/^{86}Sr_{320}$ varying between 0.707 and 0.716 (Fig. 6; Table 3). São Bartolomeu do Outeiro meta-felsic rocks also have model ages of approximately 1.1 Ga, whereas the meta-felsic rock from the Viana Dam sector (PMT-12 A) has the lowest model age of all analysed meta-felsic rocks, with approximately 800 Ma (Table 3). In turn, the Oriola's meta-felsic rocks show strongly negative εNd_{320} values, varying between −10.1 and − 11.8, and very enriched $^{87}Sr/^{86}Sr_{320}$ values between 0.732

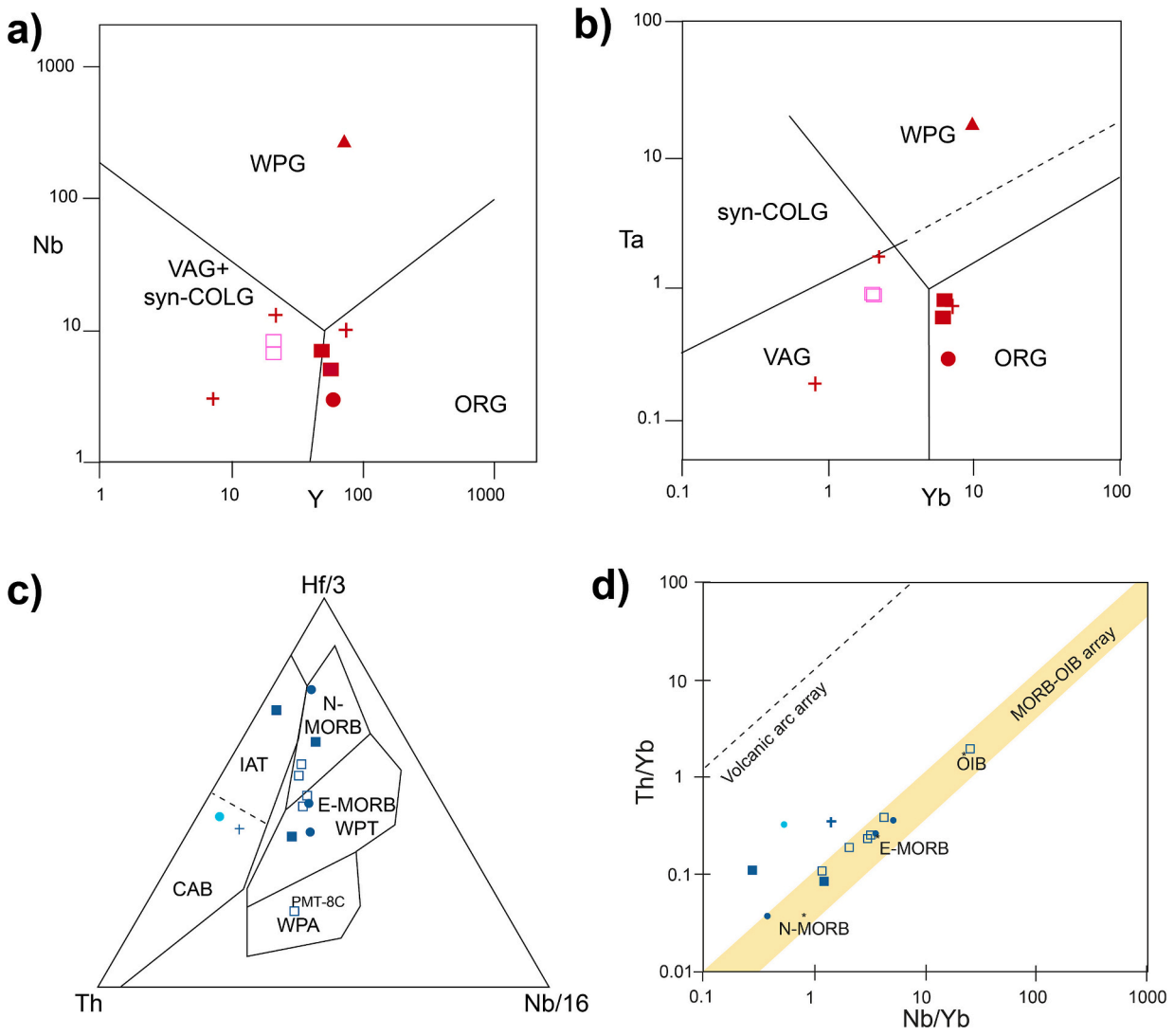

Fig. 5. – a) Nb vs Y discriminant diagram for meta-felsic samples (Pearce et al., 1984); b) Ta vs Yb discriminant diagram for meta-felsic samples (Pearce et al., 1984); c) Hf/3 - Th - Nb/16 discriminant diagram (Wood, 1980) for the meta-mafic rocks; d) Th/Yb vs Nb/Yb discriminant diagram (Pearce, 2008) for the meta-mafic rocks.

Table 3
Rb—Sr and Sm—Nd isotopic data obtained in meta-felsic and metamafic rocks of Évora-Aracena Metamorphic Belt. SW OMZ (i = 320 Ma).

Sample	Rock Type	$^{87}Rb/^{86}Sr$	$^{147}Sm/^{144}Nd$	$^{87}Sr/^{86}Sr$	error 2σ (10^{-6})	$^{143}Nd/^{144}Nd$	$^{145}Nd/^{144}Nd$	error 2σ (10^{-6})	εNd_i	T_{DM2}
PMT-1	Meta-Felsic Rocks	8.6	0.08	0.7818	11	0.511873	0.348405	6	−10.1	1827
PMT-2		2.8	0.1	0.7448	19	0.511824	0.348393	6	−11.8	1959
PMT-3		0.34	0.08	0.709	–	0.512354	0.348394	7	−0.7	1091
PMT-5		0.774	0.11	0.7193	5	0.512375	0.348402	4	−1.5	1155
PMT-12A		0.184	0.15	0.7103	6	0.512703	0.348414	6	3	800
GDW-19		5.358	0.1	0.7353	7	0.512207	0.348406	2	−4.6	1402
GDW-21		9.434	0.11	0.7796	9	0.512207	0.348414	1	−5	1433
GDW-25		0.64	0.13	0.7121	7	0.512272	0.348402	3	−4.5	1388
PMT-4	Metamafic Rocks	0.005	0.16	0.707	6	–	–	–	–	–
PMT-6		0.012	0.12	0.7073	6	0.512913	0.348403	3	8.6	364
PMT-7		0.064	0.13	0.709	6	0.512852	0.348403	4	7.1	477
PMT-8C		0.00004	0.08	0.7051	7	0.512604	0.348413	2	4.1	717
PMT-9A		0.003	0.15	0.7058	4	0.512905	0.348406	2	7.3	467
PMT-9B		0.002	0.16	0.7058	4	0.512967	0.348398	2	7.9	416
PMT-9C		0.034	0.2	0.7089	4	0.513081	0.34804	2	8.5	367
PMT-11		0.009	0.17	0.7081	5	0.513031	0.348409	4	8.9	340
PMT-12B		0.058	0.19	0.712	6	0.512773	0.348406	4	2.9	811
PMT-13		0.00003	0.12	0.7065	4	0.512835	0.348408	3	7.1	481
PMT-14		0.007	0.11	0.706	5	0.512815	0.348403	5	7.2	470
PMT-16		0.003	0.22	0.7066	5	–	–	–	–	–
GDW-26		0.134	0.17	0.7088	7	0.512697	0.348403	3	2.2	867

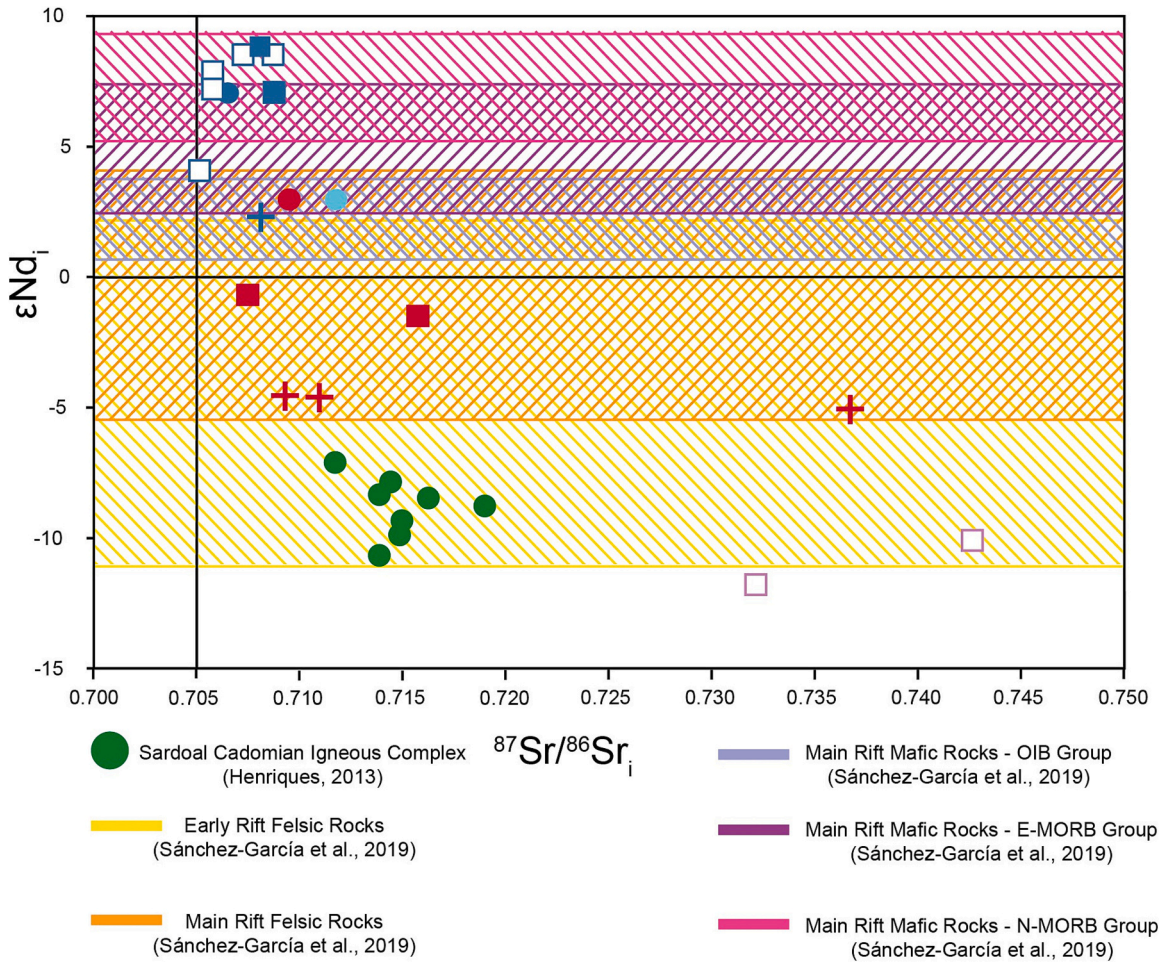

Fig. 6. – εNd_i vs $^{87}Sr/^{86}Sr_i$ diagram of the studied samples (i = 320 Ma) and comparison with similar Late Ediacaran (Henriques, 2013) and Cambrian meta-felsic and meta-mafic rocks (Sánchez-García et al., 2019) from the OMZ.

and 0.743 (Fig. 6; Table 3). Concordantly, these meta-felsic rocks also have the oldest model ages (T_{DM2} = 1.83–1.96 Ga; Table 3). As for the meta-felsic rocks from the Aracena Massif, these samples display intermediate model ages (1.39–1.43 Ga) and εNd_{320} values (−4.5 to +5.0) compared to the previous two groups, with $^{87}Sr/^{86}Sr_{320}$ values varying between 0.709 and 0.737 (Fig. 6; Table 3).

Meta-mafic rocks have relatively close εNd_i values to each other (εNd_{320} = +7.1 to +8.5 and $^{87}Sr/^{86}Sr_{320}$ = 0.703–0.709), except for samples PMT-8C (εNd_{320} = +4.7), PMT-12B (εNd_{320} = +2.9) and GDW-26 (εNd_{320} = +2.2), which present significantly lower values (Fig. 6; Table 3). Typically, model ages are not calculated for mafic rocks because results are very close to its formation age, hence precluding a real crustal evolution. However, because obtaining absolute ages for the mafic rocks proved challenging (see next section), to be able to compare with the model ages of the meta-felsic samples, these values were also calculated for the meta-mafic counterparts. These meta-mafic rocks have model ages that mainly vary between 340 and 480 Ma, with only samples PMT—12B, GDW-26 and PMT-8 showing older T_{DM2} ages of 811, 866 and 716 Ma, respectively (Table 3). Interestingly, both εNd_{320} and model ages of the meta-mafic rock PMT-12B and the meta-felsic rock PMT-12 A, that occur side-by-side in the field, are nearly identical (Fig. 6; Table 3).

7. LA-ICP-MS zircon geochronology

Four meta-felsic samples, two from the Viana do Alentejo region (one from Portel-São Lourenço sector and one from Oriola sector) and two from the Aracena Massif, as well as two meta-mafic rocks (both from the Viana Dam sector in the Viana do Alentejo region) were subjected to U—Pb zircon analysis by in situ LA-ICP-MS.

7.1. Meta-felsic rocks

Oriola's rhyolite zircons (PMT-2) are commonly elongated with bipyramidal terminations (Fig. 7a). The Th/U values in these zircons range from 0.02 to 4.25 and U contents vary between 47 and 476 ppm. Of 127 spots analysed, 110 show concordant ages (Supplement table 1 and 2). The majority of $^{206}Pb/^{238}U$ ages range from 500 to 718 Ma (Fig. 7b), with a cluster of four late Ediacaran ages, ranging between 541 and 551 Ma (Fig. 7c), yielding a weighted mean age of 546.4 ± 4.5 (Fig. 7d; n = 4; MSWD = 1; p = 0.38), that appears to represent the best estimate for the crystallization age. A few ages below 550 Ma are plotted below the Concordia line, suggesting that those youngest ages are the result of partial radiogenic Pb loss. The majority of older $^{207}Pb/^{235}U$ ages are Paleoproterozoic (1704–2187 Ma), with two analyses revealing an Archaean age (2510 and 2849 Ma; Fig. 7b). The Mesoproterozoic is weakly represented, with only six ages ranging from 1032 to 1572 Ma (only three of them concordant), and a small Tonian signal, with ages between 731 and 942 Ma, is observed.

Zircons from sample GDW-21, in the Aracena Massif, are slightly elongated with bipyramidal terminations (Fig. 8a). Sample GDW-21 presents Th/U values between 0.01 and 0.72 and U contents vary between 36.9 and 942.2 ppm. Of 83 spots examined, with 50 show concordant ages (Supplement table 3). Most (32) of $^{206}Pb/^{238}U$ ages

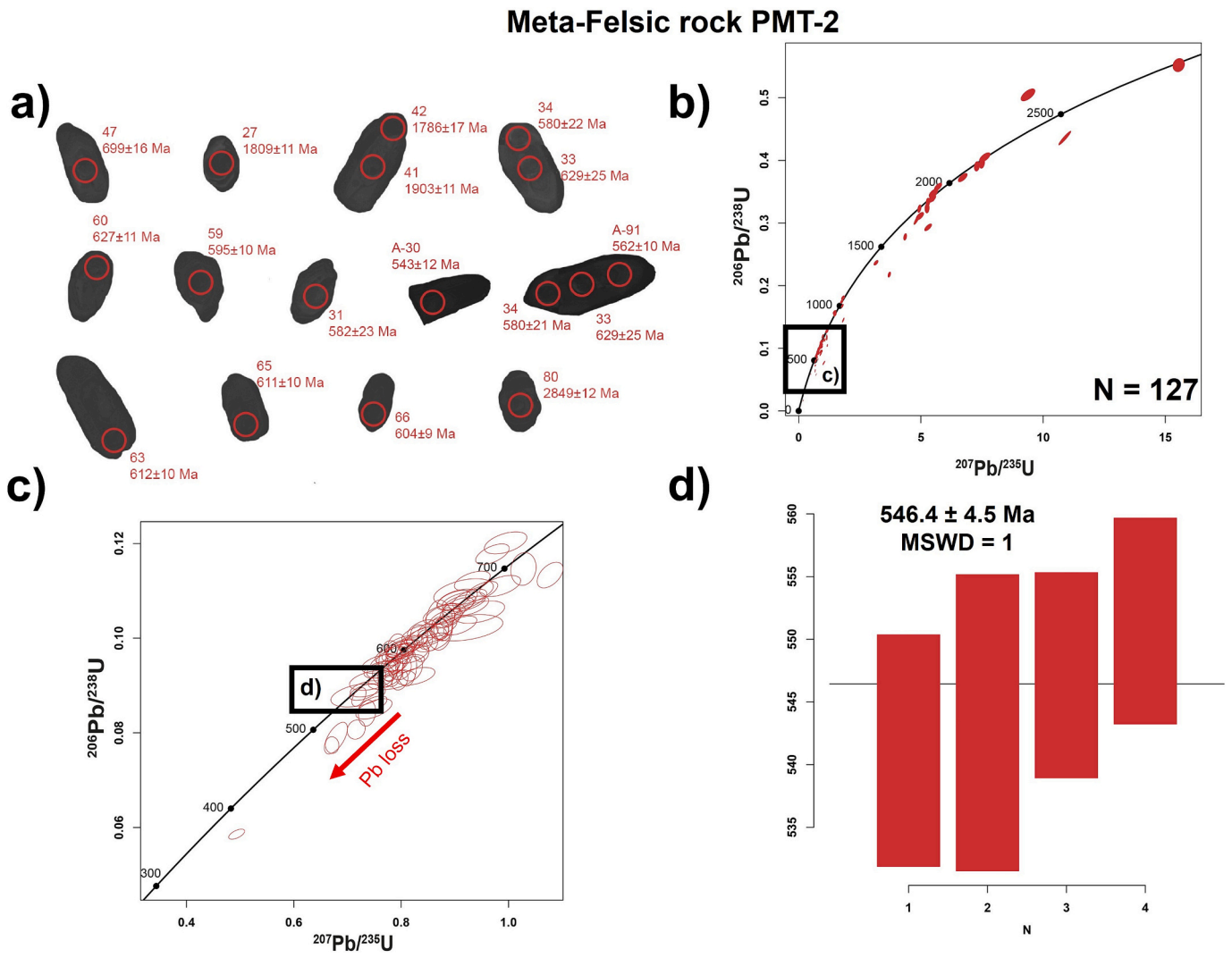

Fig. 7 – U-Pb. geochronological results of meta-felsic sample PMT-2: a) Scanning electron microscope (SEM) cathodoluminescence (CL) images of representative zircon grains; b) Wetheril Concordia diagram showing the entire set of LA-ICP-MS analyses; c) Wetheril Concordia diagram between 300 and 700 Ma; and d) $^{238}U/^{206}Pb$ ages weighted mean average diagram for analyses between 550 and 650 Ma.

range from 496 to 581 Ma (Fig. 8b). A cluster of nine late Ediacaran to mostly Cambrian ages, ranging between 540 and 517 Ma (Fig. 8c), yields a weighted mean age of 525.0 ± 2.2 (Fig. 8d; $n = 8$; MSWD = 1.1; $p = 0.33$), that appears to represent the best estimate for the crystallization age. The oldest ages are Neo-Archean (2577 and 2630 Ma), with a Tonian age cluster (705–759 Ma) and an Ediacaran-Cryogenian cluster (600–652 Ma) also being observed (Fig. 8b). The youngest age obtained in sample GDW-21 is of Tournaisian age (349 Ma), with an Ordovician cluster (446–479 Ma) also observed.

Zircons from Portel-São Lourenço meta-felsic rock (PMT-17) have sub-rounded morphologies with a few elongated prismatic zircons with bipyramidal terminations (Fig. 9a). These zircons exhibit a Th/U range of 1.2 to 4.0 and highly variable U contents (44–1295 ppm). 20 spots were examined, 19 of which produced concordant ages (between 90 and 110 % concordance; Supplement table 4). The majority of $^{206}Pb/^{238}U$ ages range from 502 to 679 Ma (Fig. 9b and c). The youngest cluster shows a Concordia age of 504.15 ± 1.98 Ma (Miaolingian; Fig. 9d; $n = 3$; MSWD = 0.25; $p = 0.62$), which is interpreted as the crystallization age. The clusters at 613 and 672 Ma are also significant. Several analyses also produced Late Palaeozoic (321 Ma) to Mesozoic $^{206}Pb/^{238}U$ ages (227–232 Ma). $^{207}Pb/^{235}U$ ages of the Mesoproterozoic (1521 Ma), Paleoproterozoic (1836 and 2057 Ma), and Archaean (2806 Ma) were also obtained.

As for sample GDW-25, zircons are slightly elongated with bipyramidal terminations (Fig. 10a), while Th/U values vary between 0.20 and 0.97 and U contents range from 212 to 1008 ppm. A total of 52 spots were examined, with 31 showing concordant ages (Supplement table 5). 30 of these $^{206}Pb/^{238}U$ ages range from 462 to 523 Ma (Fig. 10b and c), with a cluster of 14 Furongian to Lower Ordovician ages, between 488 and 473 Ma, giving the best estimate at a crystallization age of 481.9 ± 1.5 (Fig. 10d; $n = 14$; MSDW = 9.4; $p = 0.0022$). The youngest analysis has a Rhuddanian age (441 Ma).

7.2. *Meta-mafic rocks*

The zircons from the two meta-mafic rocks, cropping out in the Viana Dam sector, frequently feature a rounded shape, with occasional prismatic morphology (Fig. 11a). Th/U values range between 0.02 and 3.08 and U contents between 18 and 378 ppm. A total of 40 spots were analysed (38 from sample PMT-12B – Supplement table 6 and 7 - and 2 from PMT-16 – Supplement table 8), 22 of which display concordant ages. The two core analysis from sample PMT-16 yielded $^{207}Pb/^{235}U$ Mesoproterozoic ages, respectively 1047 ± 17 Ma and 1070 ± 19 Ma, without further information being available, therefore precluding any interpretation. In sample PMT—12B, although the youngest spot analysis presents a lower Mississippian $^{206}Pb/^{238}U$ age (354 ± 8 Ma),

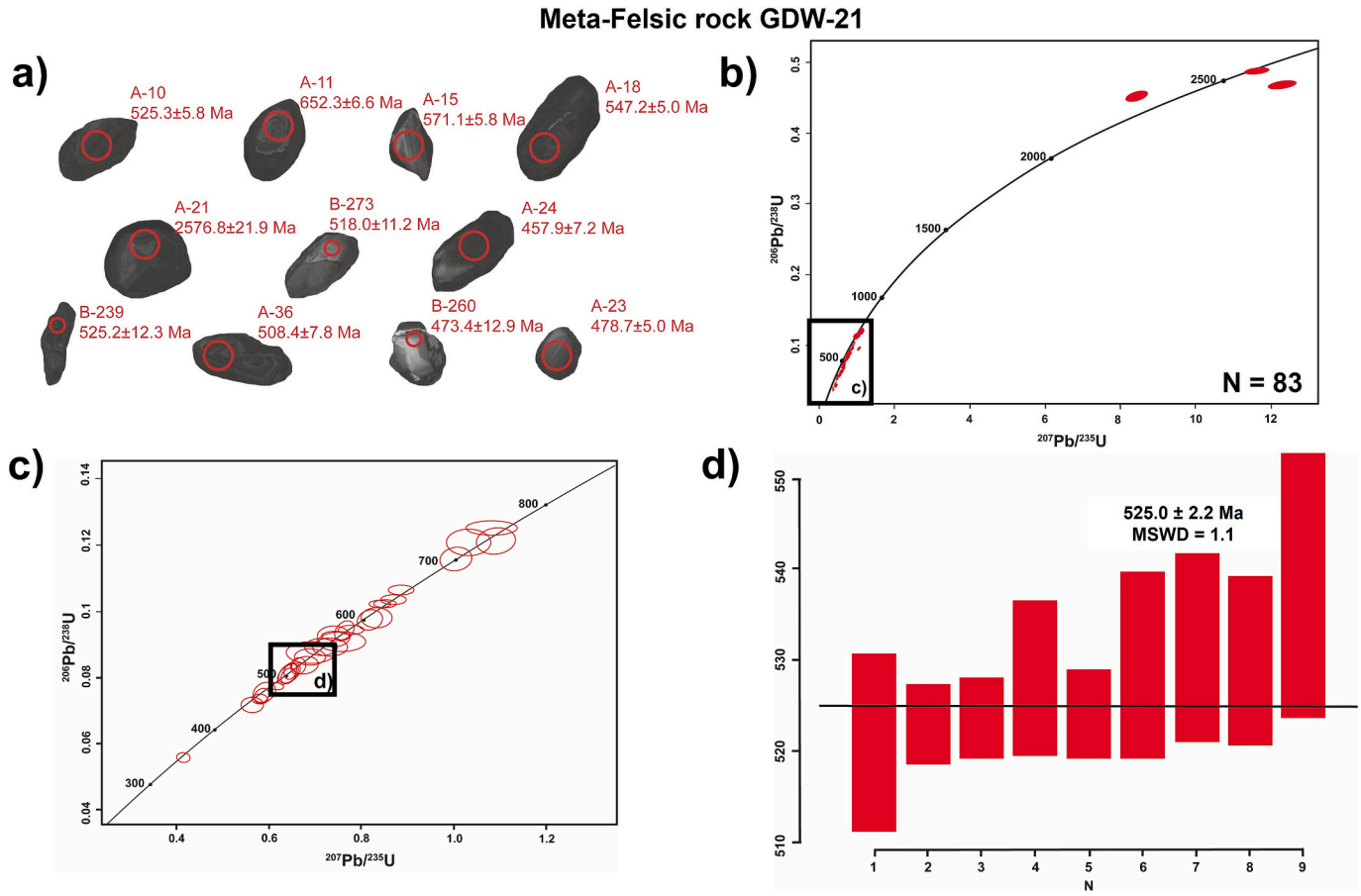

Fig. 8 – U-Pb. geochronological results of meta-felsic sample GDW-21: a) Scanning electron microscope (SEM) cathodoluminescence (CL) images of representative zircon grains; b) Wetheril Concordia diagram showing the entire set of LA-ICP-MS analyses; c) Wetheril Concordia diagram between 300 and 800 Ma; and d) $^{238}U/^{206}Pb$ ages weighted mean average diagram for analyses between 517 and 540 Ma.

probably due to radiogenic Pb loss during a Variscan thermal event. Most of the $^{206}Pb/^{238}U$ ages range between 542 and 714 Ma (Fig. 11b and c). The pattern of ages closely resembles a detrital sediment. The youngest cluster shows weighted mean age of 555.8 ± 5.3 Ma (n = 3; MSWD = 5.5; p = 0.004; Fig. 11d), which is considered the best conservative approximation of the crystallization age or of the maximum deposition age (MDA) depending on whether the sample is igneous or a volcanoclastic rock. Nonetheless, we acknowledge that the zircons in this cluster, although being concordant (with concordances ranging from 94 to 96 %), are positioned somewhat below the Concordia, which could indicate an even older crystallization date, presumably a ~ 600 Ma, where two extremely concordant zircons are located. The oldest concordant cluster is Paleoproterozoic with $^{207}Pb/^{235}U$ ages ranging from 2108 to 1907 Ma. The Mesoproterozoic is almost absent, being represented by mostly non-concordant ages ranging between 1050 Ma and 1350 Ma.

8. Discussion

8.1. Petrogenesis of the meta-felsic rocks

As previously mentioned, Sr—Nd isotopic data obtained in the studied meta-felsic rocks shows a large spectrum of model ages and εNd, just like most Cambrian Rift-to-Drift felsic rocks (Fig. 6; Sánchez-García et al., 2019). On one end of the spectrum, meta-felsic rocks from Oriola have the oldest model ages, from 1.8 to 1.96 Ga (Table 3), likely associated with the Birimian event of the Eburnean Orogeny (Lemoine et al., 1990). Oriola's meta-felsic rocks also present extremely negative εNd_{320} values (−10.1 to −11.8), suggesting an upper crust source (Fig. 6). Such extremely negative εNd values have also been describes both for Cadomian-related rocks (Henriques, 2013) and felsic rocks formed in the early stages of the Cambrian Early Rift event (Sánchez-García et al., 2010). On the other end, meta-felsic rocks from São Bartolomeu do Outeiro and Viana Dam sectors present younger model ages, around 1.1 Ga (Table 3), which can be associated with a later event, namely the Grenvillian Orogeny, related to the formation and dismantling of the supercontinent Rodinia (1.4 Ga - 900 Ma; e.g.: Fitzsimons, 2000; Meert, 2001; Condie, 2002). Considering the absence of Grenvillian events in the OMZ, these T_{DM2} are most likely the result of source mixture from the Eburnean Orogeny and other younger magmatic events, like the Pan-African/Cadomian Orogeny (e.g.: Eguíluz et al., 2000; Linnemann et al., 2007, 2008a, 2008b), the Cambrian rifting events (e.g. Sánchez-García et al., 2010, 2014, 2019) or even the Variscan Orogeny itself (e.g.: Díaz-Azpiroz et al., 2006; Pereira et al., 2009). Meta-felsic rocks from São Bartolomeu do Outeiro also present significantly less negative εNd values (Fig. 6), with Viana Dam sample displaying slightly positive values, which points to a deeper source. Such slightly negative to positive εNd values have also been observed in felsic rocks generated at a more advanced stage of the Cambrian Early Rifting event (e.g.: Sánchez-García et al., 2014).

This difference between Oriola's meta-felsic rocks and São Bartolomeu do Outeiro and Viana Dam meta-felsic rocks is also evident in the geochemistry data. Meta-felsic rocks from São Bartolomeu do Outeiro and Viana-Dam sectors are more enriched in HREE (Fig. 4a), while also showing an anorogenic signature on the diagram after Pearce et al. (1984); Fig. 5a and b). This anorogenic signature, together with higher εNd_{320} values, suggests that São Bartolomeu do Outeiro and Viana Dam meta-felsic rocks were most likely generated during the Cambrian

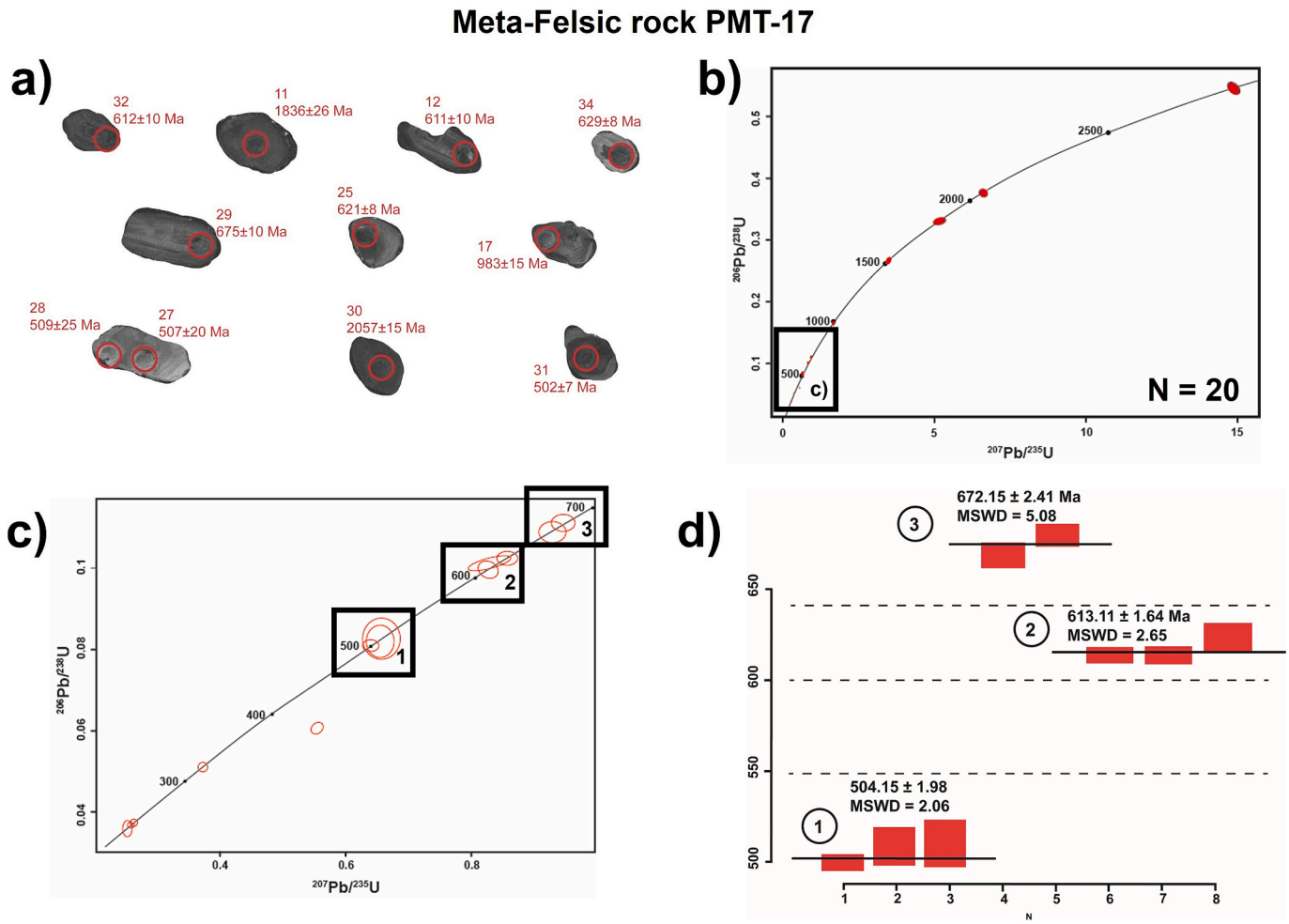

Fig. 9 – U-Pb. geochronological results of meta-felsic sample PMT-17: a) Scanning electron microscope (SEM) cathodoluminescence (CL) images of representative zircon grains; b) Wetheril Concordia diagram showing the entire set of LA-ICP-MS analyses; c) Wetheril Concordia diagram between 300 and 700 Ma; and d) $^{238}U/^{206}Pb$ ages weighted mean average diagram for analyses between 500 and 700 Ma.

magmatic pulses ("Early Rift event" of Sánchez-García et al., 2010, 2014, 2019). In contrast, Oriola's meta-felsic rocks present an orogenic signature (Fig. 5a and b) and display significantly more depleted HREE patterns (Fig. 4a). Geochronological data obtained in one of Oriola's meta-felsic rocks (PMT-2) indicates an Ediacaran crystallization age, with an estimated weighted mean age ca. 546.4 ± 4.5 Ma. The ca. 601 to 699 Ma age interval continuum (Fig. 7c) likely reflects an igneous zircon inheritance and coincides with one of the most productive (most active thermal/magmatic pulses) of the long-lived Pan-African orogenic event (Black et al., 1994; Bento dos Santos et al., 2015; Chichorro et al., 2022). This evidence strongly suggests that the older, probably Pan-African igneous rocks, are participating as melting sources for the Cadomian magmatism. Oriola's meta-felsic rocks also seem to have been affected by the later Cambrian event, as the Concordia diagram for sample PMT-2 also shows non-concordant younger ages (Fig. 7c) that we interpret as an ensuing thermal isotopic destabilization that promoted Pb loss and consequent decrease of the influence of the main Ediacaran age. Since these Cambrian ages terminate in a quasi-concordant ~500 Ma cluster, we link the radiogenic Pb loss to the Rift-to-Drift related Cambrian thermal event, concomitant with the timing of rift-related magmatism described in the adjacent Montemor-o-Novo Sector (Chichorro et al., 2008). However, the melting temperature was likely very low, with no formation of new zircon, but providing Pb loss to already crystallized grains.

Although no isotopic data were obtained from the Portel-Sao Lourenço meta-felsic rocks, this sample denotes a more significant enrichment in REE than the others (Fig. 4a), as well as a greater enrichment in Nb (Fig. 4c), depicting an anorogenic signature (Fig. 5a and b). Such geochemical characteristics imply a more significant mantle influence, with the U—Pb data (crystallization age of 504 Ma) supporting a later genesis, well within the main rift stage (Sánchez-García et al., 2019; Cachapuz et al., 2024). As this sub-volcanic rhyolite is included within the Moura Phyllonitic Complex, it points to a minimum Cambrian (Wuliuan/Drumian transition) age for this unit, contrary to the upper Ordovician to lower Devonian age (Piçarra, 2000) that had previously been suggested for the Moura Phyllonitic Complex and assumed in Geological regional map; (Ferreira and Piçarra, 2020). Other clusters, at around 613 and 672 Ma (Fig. 9c and d), are most likely inherited and linked to Pan-African igneous crust is being incorporated in Rift-to-Drift melts (as described in Chichorro et al., 2022). Older inheritances (Mesoproterozoic, Paleoproterozoic and Archaean ages) are likely related to ancient thermal events recorded on the source region of these magmas. A concordant Late Palaeozoic Pennsylvanian age is also present (Fig. 9c), possibly representing an independent stage of zircon precipitation during Variscan metamorphism, as described for the second peak of granitoid emplacement in the Évora Massif at ca. 320–317 Ma (Pereira et al., 2009; Moita et al., 2015).

As for Aracena's meta-felsic rocks, these present intermediate model ages (1.39–1.43 Ga) and εNd_i values (−4.5 to −5.0) compared to the remaining meta-felsic rocks, suggesting that these rocks result from hybrid melts with a mix of supra and infracrustal sources. Such source mixing would explain the heterogeneity of geochemical features

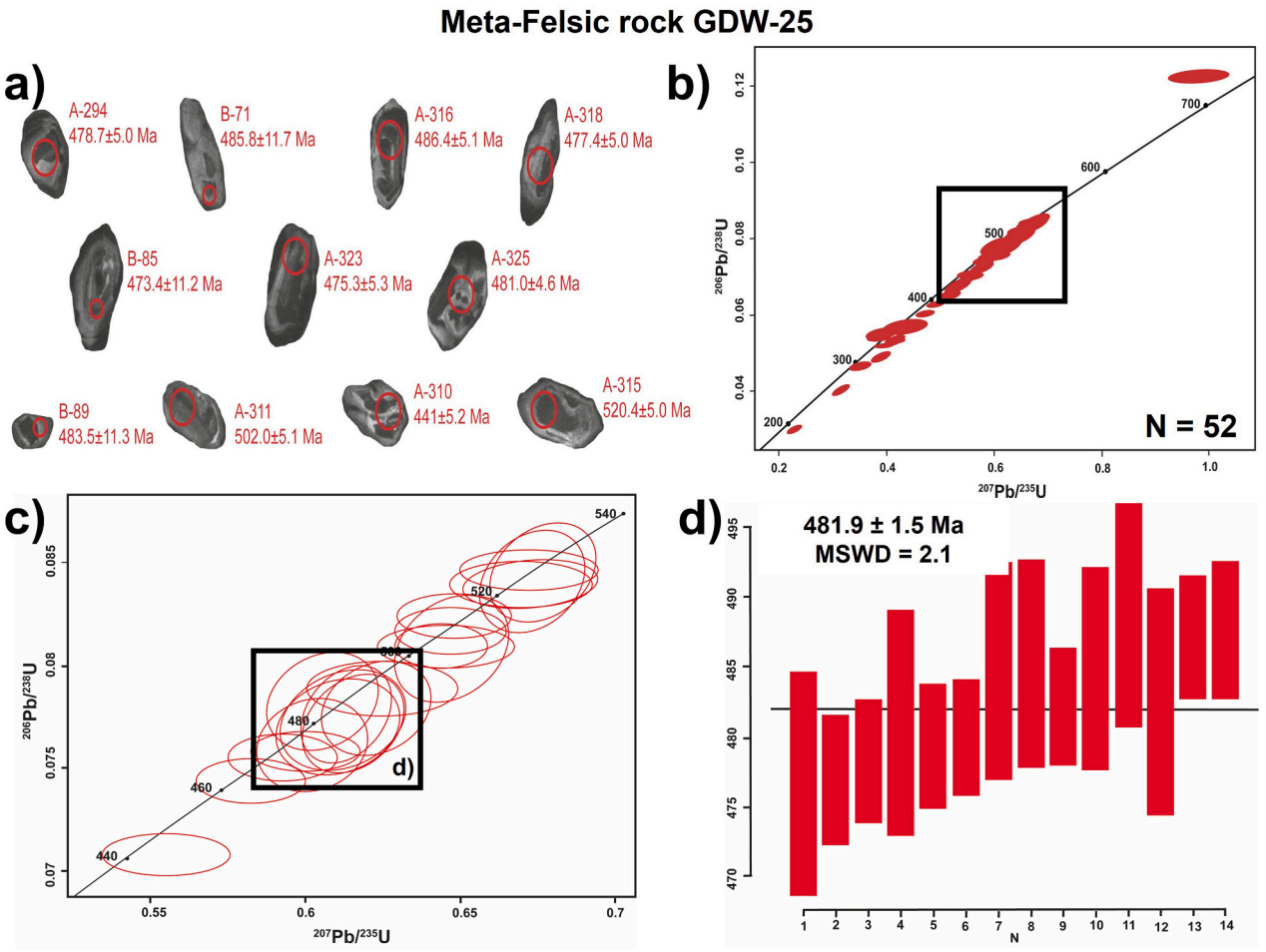

Fig. 10 – U-Pb. geochronological results of meta-felsic sample GDW-25: a) Scanning electron microscope (SEM) cathodoluminescence (CL) images of representative zircon grains; b) Wetheril Concordia diagram showing the entire set of LA-ICP-MS analyses; c) Wetheril Concordia diagram between 440 and 540 Ma and d) $^{238}U/^{206}Pb$ ages weighted mean average diagram for analyses between 470 and 500 Ma.

observed in the Aracena's meta-felsic rocks, as sample GDW-21 displays an orogenic signature (Fig. 5a and b) and REE pattern similar to Oriola's meta-felsic rocks (Fig. 4a), while sample GDW-19 shows a significant depletion in HREE and higher Ce/Yb values compared to Oriola's meta-felsic rocks, which might indicate a strong participation of a sedimentary source in the melting. In turn, sample GDW-25, like the São Bartolomeu do Outeiro and Viana Dam meta-felsic rocks, shows an Ocean-Ridge signature (Fig. 5a and b). However, its RE*E*-enrichment (REEt = 317 ppm; Fig. 4a) is more similar to Portel-São Lourenço rhyolite. Geochronological data obtained in these Aracena's meta-felsic rocks place sample GDW-21 in the Early Rift Event, with an age of 525 Ma. As such, it can be said that the orogenic signature and similar HREE pattern to Cadomian rocks, like the ones from Oriola sector and Sardoal Igneous Complex (Henriques, 2013) in these meta-felsic rocks, are inherited. This geochemical similarity between Ediacaran and Cambrian volcanic rocks has been described by several other authors (e.g.: Sánchez-García et al., 2014; Pereira et al., 2023) and it is typically attributed to a significant supra-crustal contribution, which caused the early Cambrian rift-related rocks to inherit some features from arc-like Cadomian-to-Pan-African rocks. This supra-crustal component is also evidenced by the strong proportion of Ediacaran ages obtained in these sample (Fig. 8c). In contrast, sample GDW-25 seems to have a more infra-crustal component, due to its anorogenic signature (Fig. 5a and b) and HREE-enriched patterns (Fig. 4a), with the geochronological data placing this sample in the Late Rift Event (Concordia age of 481.9 ± 1.5 Ma), a novelty in the SW OMZ.

In terms of magmatic evolution, the low number of samples in Oriola and Portel-São Lourenço sectors makes it virtually impossible to define any significant trends in the Harker diagrams. São Bartolomeu do Outeiro and Viana Dam meta-felsic rocks show negative correlations with Al_2O_3 and Na_2O (Appendix 2), probably due to Na-rich plagioclase fractionation, and FeO_t (Appendix 2), likely the result of Fe-oxides (e.g.: magnetite) fractionation. It is, however, important to note that only three samples define these correlations, and as such, results might be misleading, and their interpretation cannot be seen as conclusive.

8.2. *Petrogenesis of the meta-mafic rocks*

Most EAMB meta-mafic rocks denote geochemical characteristics very similar to the meta-mafic rocks associated with the Cambrian (Series 2 – Miaolingian) magmatic event, the Main Rift stage (e.g.: Araújo et al., 2005; Chichorro et al., 2008; Pedro et al., 2010; Sánchez-García et al., 2010), which have a sub-alkaline character (Appendix 1b and c) and an anorogenic signature, varying between N-MORB and E-MORB affinity (Fig. 5c and d). The EAMB's meta-mafic rocks are characterized by high variability of $(La/Lu)_N$ ratios (Fig. 4b), ranging from LREE enriched patterns, typical of E-MORB, to HREE enriched patterns, often associated with N-MORBs. There are three possible causes for this $(La/Lu)_N$ variability: i) fractional crystallization; ii) different degrees of crustal contamination; or iii) heterogeneity in the mantle source.

The linear trend in the $(La/Lu)_N$ vs #Mg diagram (Fig. 12a) shows a correlation between the variation of the $(La/Lu)_N$ ratios and the evolution of the meta-mafic rocks, thus confirming that fractional crystallization processes had a significant role in the $(La/Lu)_N$ variability, just as

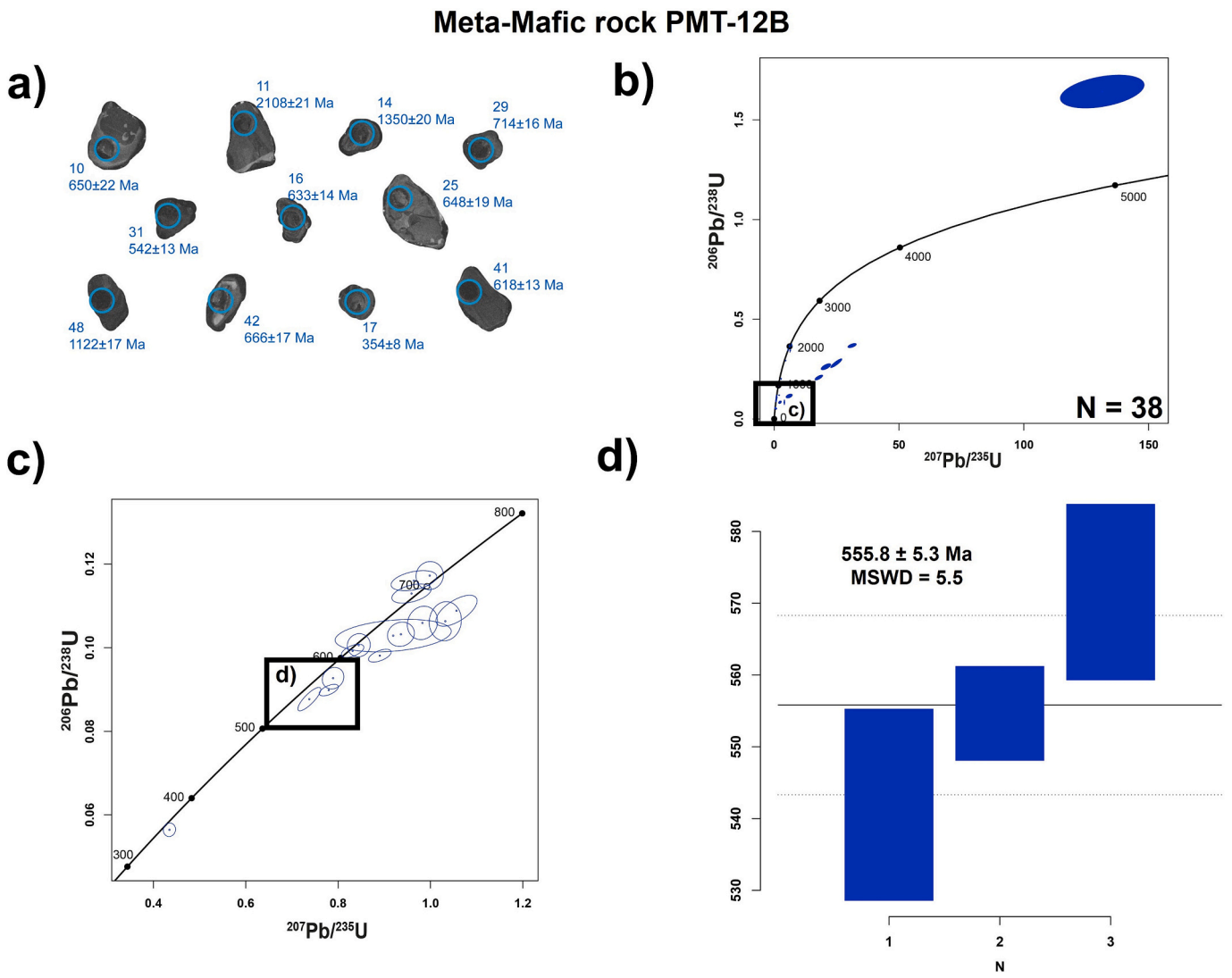

Fig. 11 – U-Pb. geochronological results of meta-mafic sample PMT—12B: a) Scanning electron microscope (SEM) cathodoluminescence (CL) images of representative zircon grains; b) Wetheril Concordia diagram showing the entire set of LA-ICP-MS analyses; c) Wetheril Concordia diagram between 300 and 700 Ma; and d) $^{238}U/^{206}Pb$ ages weighted mean average diagram for analyses between 530 and 580 Ma.

proposed by Castro et al. (1996). Harker diagrams for these meta-mafic rocks show negative correlations with CaO, Al_2O_3 and MgO (Appendix 2). Ca-rich plagioclase fractionation could account for CaO and Al_2O_3 correlations, whereas pyroxene fractionation would be responsible for MgO correlation. Ca-rich plagioclase fractionation is also evident from the negative trend shown by Sr, which tends to replace Ca in the plagioclase. This pyroxene and plagioclase fractionation suggests that the meta-mafic rocks resulted from more evolved magmas.

Regarding the possibility of crustal contamination, LILE enrichment and positive Pb and K anomalies (typically enriched in the crust), as well as negative P and Nb anomalies (typically depleted in the crust) suggest that the studied mafic rocks were subjected to different degrees of crustal contamination. However, a more detailed analysis shows that these rocks have K/P ratios below 7 and Ti/Yb ratios above 1000 (Table 2). These values are typical of uncontaminated samples (Brueseke and Hart, 2009). Some samples have $K/P > 7$, which is probably associated with a late remobilization event during the Variscan metamorphism, given the high mobility of these two elements, particularly K.

As for mantle heterogeneity, most meta-mafic rocks from the EAMB appear to come from the same region of the mantle (spinel peridotite region; Fig. 12b), although with varying degrees of enrichment (as evidenced in Fig. 12c). There are, however, three exceptions, namely samples PMT—12B, GDW-26 and PMT—8C. The latter appears to come from a shallower, more depleted source (garnet peridotite region), while the first 2 samples plot in the lithospheric mantle field. Such existence of more than one mantle source for mafic rocks of the OMZ had already been described in the Montemor-Ficalho Sector (e.g.: Pedro et al., 2010).

Samples PMT—12B, PMT-8C and GDW-26 not only have different sources relative to the remaining meta-mafic rocks, but also different signatures and isotopic values. Samples PMT-12B and GDW-26 show a subduction-related basalts signature (CAB; Fig. 5c), whereas sample PMT-8C displays a within plate signature. Samples PMT-12B and GDW-26 also plot outside the MORB-OIB array (Fig. 5d). Furthermore, all three samples also have lower εNdi values relatively to the majority of meta-mafic rocks from the EAMB, with PMT-12B and GDW-26 displaying relatively close values to the PMT-12 A rhyolite (Fig. 6).

If the PMT-12B amphibolite represents an igneous protolith, the geochronological data suggest a Neoproterozoic age (555.8 ± 5.3 Ma or even older Ediacaran age), significantly younger than the age obtained by Akker et al. (2020) in mafic rocks of Viana do Alentejo region (815–790 Ma), and confirming the presence of Cadomian mafic rocks in the region, as previously suggested by Rosas et al. (2008), which would justify its crustal signature within the Cadomian magmatic arc. The geochronological and geochemical characteristics of this amphibolite

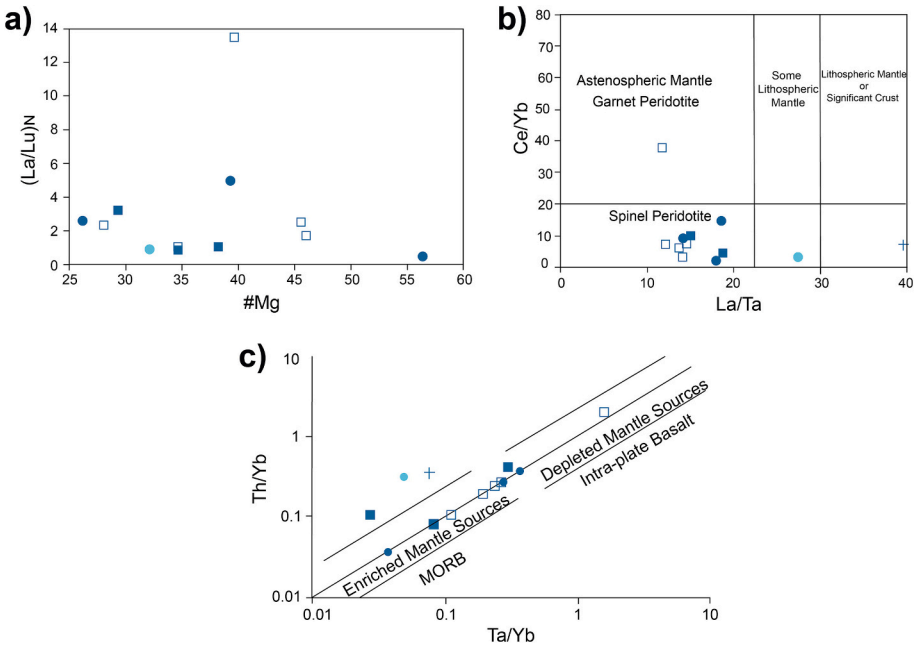

Fig. 12. – Inferences on geochemical processes for the studied meta-mafic samples: a) La/Lu_N vs #Mg diagram; b) Ce/Yb vs La/Ta diagram; and c) Th/Yb vs Ta/Yb diagram. Adapted from Pearce (1982) and Wilson (1989).

are in all similar to Group 3 metabasites of Sánchez-Lorda et al. (2014, 2016). Alternatively, this Ediacaran age may also represent an MDA obtained on a volcanoclastic mafic protolith that incorporated a *syn*-volcanic Cadomian arc component.

This means that, during the Neoproterozoic-Cambrian transition, there were two periods of mafic magmatism in SW OMZ, one during the Cadomian Orogeny and another during the Cambrian rifting event. This is also supported by the T_{DM2} ages, with samples PMT-12B and PMT-8C (811 and 716 Ma, respectively; Table 3) presenting significantly older ages than the remaining meta-mafic rocks (T_{DM2} = 340–480 Ma; Table 3). Although no U—Pb data were obtained, this appears to suggest that sample PMT-8C was also formed in an earlier stage when compared to most mafic magmatic rocks of the Viana do Alentejo region.

8.3. Geodynamic context

The geochemical and geochronological data acquired in this study indicate the existence of both mafic and felsic magmatism linked to the Cadomian Orogeny, representing an important finding in the EAMB. As mentioned above, Cadomian-related meta-felsic rocks display very similar geochemical characteristics to rocks generated in the earlier stages of the Early Rift event. This is probably the consequence of the melting of a supra-crustal component during the initial phases of the Cambrian rifting event (e.g.: Sánchez-García et al., 2010).

Our data also suggest that the change from a subduction-to-collision setting to a Rift-to-Drift setting, during the late Ediacaran – early Cambrian, occurred in a continuous manner, both in terms of geochemistry (as both Ediacaran and early Cambrian meta-felsic rocks have very similar geochemical characteristics) and geochronology. This gradual transition is evident when looking at the geochronological data obtained in sample GDW-21, generated during the Early Rift event with a crystallization age of 525 Ma, where most concordant zircons (almost 50 %) form a cluster of ages between 600 and 500 Ma (Fig. 8c), with no clear gaps. This suggests that the transition from the end of the Cadomian collision to the early stages of the Rift event was progressive, with a succession of multiple magmatic pulses (as noticed by Simancas et al., 2004). The absence of a substantial gap between the Cadomian collision and the Early Rift event is also evidenced in the geochronological data from sample PMT-2, from Oriola, where, despite its Ediacaran age (~546 Ma), there are a few younger slightly non-concordant zircons with Cambrian ages (Fig. 7c).

The question that arises is what caused this transition from an arc setting to a rifting environment. In our view, the subduction of a mid-ocean ridge beneath the continental crust, as proposed by Sánchez-García et al. (2003, 2008, 2010), is likely the mechanism to trigger this convergent to divergent transition (Fig. 13). This subduction of a mid-ocean ridge would cause the opening of a slab window, in turn, causing the thermal expansion of the upper continental crust and subsequent gravitational collapse. As such, magmatism in the Early Rift event would mainly derive from crust partial melting, with reduced mantle influence, which in turn would justify the geochemical similarities between Cadomian and Early Rift magmatic rocks. This model of ridge subduction as the cause of rifting inception during the Cambrian fits well with the evidence of gradual opening of the magmatic system to tholeiitic *E*- to N-MORB magmas. Similar mechanisms of ridge-trench interactions have been assumed for other portions of the Avalonian–Cadomian belt, namely in Teplá–Barrandian unit, Bohemian Massif (Hajná et al., 2018). Linnemann et al. (2007) also proposed the subduction of a mid-ocean ridge accompanied by slab break-off of the subducted crust to justify this transition to a rifting environment. The increase in the angle of the subduction after eclogitization of the subducted slab, as proposed by Arenas et al. (2007) and Moreno-Martín et al. (2023), could also lead to the same modification of the geodynamic setting, and similar opening of the system to tholeiitic MORB magmas. The same can be said of the upwelling of a mantle plume (e.g.: Winchester et al., 2006). However, further discussion on this topic is out of scope for our study. These models must be checked against numerical modelling data and further geochronological data to test their overall soundness.

As rifting advanced, mantle influence grew (e.g.: Sánchez-García et al., 2010; 2014). This greater influence is evident in the geochemistry of the meta-felsic rocks from the later stages of the Early Rift event, such as those from São Bartolomeu do Outeiro and Viana Dam, which exhibit notably younger model ages (Table 3), fewer negative εNd values (Fig. 6), and anorogenic signatures (Fig. 5a and b). However, the increase in mantle-derived material is mainly noted during the Main Rift event. Not only do Main Rift meta-felsic rocks, such as PMT-17, have unique geochemical properties, namely a pronounced enrichment in

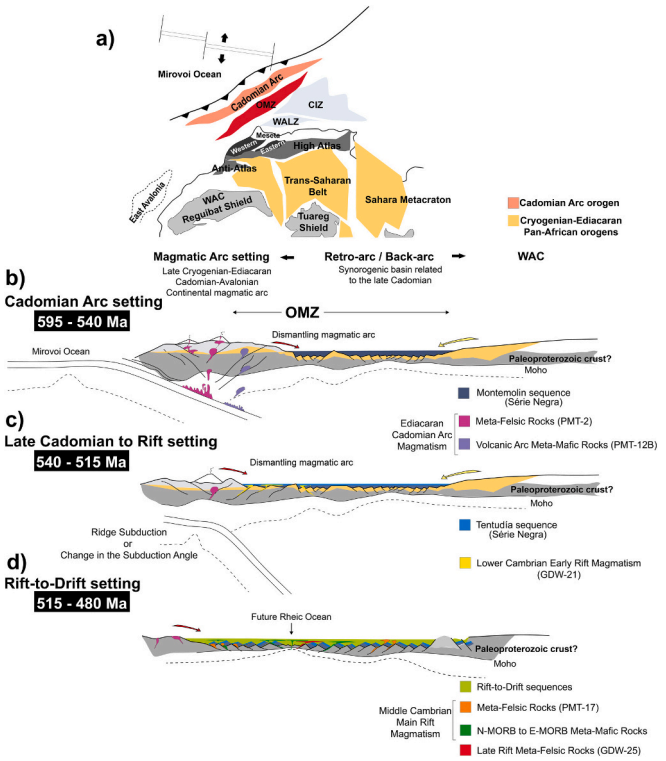

Fig. 13. – Proposed paleogeographic reconstruction of Ossa Morena Zone within Gondwana's northern margin during the Neoproterozoic-Early Cambrian (a); and its schematic evolution from Neoproterozoic subduction-collision (subduction of the Mirovoi ocean – Sánchez-García et al., 2019) to the Cambrian-Ordovician Rift event (b to d) that led to the opening of the Rheic ocean (Sánchez-García et al., 2003, 2008, 2010) as mentioned in the text. OMZ - Ossa Morena Zone, WALZ - West Asturian-Leonese Zone, CIZ - Central Iberian Zone, WAC - West African Craton.

REE (Fig. 4a), they are associated with mafic lithologies, which are entirely absent in the Early Rift event. As such, it can be said that the EAMB presents a remarkable magmatic record of the ~100 Ma interval between the end of the Cadomian Orogeny and the rifting processes that led to the opening of the Rheic ocean.

9. Conclusions

Based on the obtained results for the meta-acidic and metabasic rocks of the Évora-Aracena Metamorphic Belt in SW OMZ, the following was concluded:

- The EAMB shows a great record of the transition between the Cadomian and the Variscan cycles, especially in terms of felsic magmatism. Geochronological data confirmed the presence of Ediacaran meta-felsic rocks in the EAMB, a novelty in the region. These Cadomian-related rhyolites are geochemically similar to other meta-felsic rocks formed elsewhere in the Ossa-Morena zone during the early stages of the Early Rift event, in the lower Cambrian. This rifting-related thermal event also affected some zircons in the Ediacaran meta-felsic rocks, causing Pb loss. As such, this hints that the convergent, subduction-related regime that lasted for most of the Neoproterozoic around the margins of NW Gondwana was rapidly replaced by one dominated by rifting during the Cambrian with the Ediacaran igneous rocks actively participating as melt sources for the I-type lower Cambrian rift-related magmas.

- Meta-felsic rocks, in the EAMB, formed throughout the Rift-to-Drift event display variable geochemical characteristics, resulting from a progressive involvement of mantle derived melts. The participation of such melts is evidenced by the anorogenic signatures and more primitive isotopic signatures of the upper Cambrian to lower Ordovician meta-felsic rocks, associated with the Main and Late Rift event, while meta-felsic rocks formed in the early stages of Rift-to-Drift event (Early Rift event) result from a shallower melting, consequently showing geochemical similarities with Cadomian-related meta-felsic rocks.

- The meta-mafic rocks in the EAMB were mostly formed by magmatic processes related to an extensional setting, namely the OMZ Main Rift episode during the Middle Cambrian. The high $(La/Lu)_N$ variability in these meta-mafic rocks is associated with both fractional crystallization and some source heterogeneity. However, three amphibolites present very distinct characteristics (GDW-26, PMT-12B and PMT—8C), with one of them presenting a Neoproterozoic age (~556 Ma). This means that, while most meta-mafic rocks represent a magmatic sequence formed in a Rift-to-Drift to Drift setting that culminated in ocean crust formation, some Late Neoproterozoic mafic magmatism is also represented in the SW OMZ.

CRediT authorship contribution statement

P. Cachapuz: Writing – original draft, Visualization, Validation, Methodology, Investigation, Formal analysis, Data curation, Conceptualization. **M. Chichorro:** Writing – review & editing, Validation, Supervision, Resources, Methodology, Funding acquisition, Formal analysis, Data curation, Conceptualization. **T. Bento dos Santos:** Writing – review & editing, Validation, Supervision, Resources, Methodology, Funding acquisition, Formal analysis, Data curation, Conceptualization. **D.R. Carvalho:** Validation, Methodology, Data curation. **U. Linnemann:** Validation, Methodology, Data curation. **M. Zieger-Hofmann:** Validation, Methodology, Data curation. **J. Zieger:** Validation, Methodology, Data curation. **E. Dantas:** Validation, Methodology, Data curation. **R.V. Santos:** Validation, Methodology, Data curation. **P. Moita:** Validation, Methodology, Data curation. **M. Beltrame:** Validation, Methodology, Data curation. **A.R. Solá:** Validation, Resources, Funding acquisition, Conceptualization. **M. Díaz-Azpíroz:** Validation. **C. Fernández:** Validation.

Declaration of competing interest

The authors declare that they have no known competing financial interests or personal relationships that could have appeared to influence the work reported in this paper.

Acknowledgements

The authors would like to thank Cyntia Mourão and Pedro Rodrigues from FCUL and Stéphanie Mandrou from GET-OMP for their technical help in obtaining the results, as well as Noel Moreira for all the fruitful talks on this subject.

This work was funded by the Portuguese Fundação para a Ciência e a Tecnologia (FCT) I.P./MCTES through national funds (PIDDAC) – UID/50019/2023, LA/P/0068/2020 (doi:10.54499/LA/P/0068/2020) and UID/PRR/50019/2025 (https://doi.org/10.54499/UID/PRR/50019/2025) to IDL – Instituto Dom Luíz and UIDB/04035/2020 (doi:10.54499/UIDB/04035/2020) to GeoBioTec Research Centre, for funding and support facilities. This work was also supported by FCT through PhD grant 2022.12189.BD to Pedro Cachapuz (doi:10.54499/2022.12189.BD). This is a contribution to LNEG's project PETROGEO.

We gratefully acknowledge the valuable feedback and suggestions provided by the reviewers, as well as the contributions of the editor, Federico Lucci, and the Editor-in-chief, Astrid Holzheid, all of which were instrumental in improving this manuscript.

Appendix A

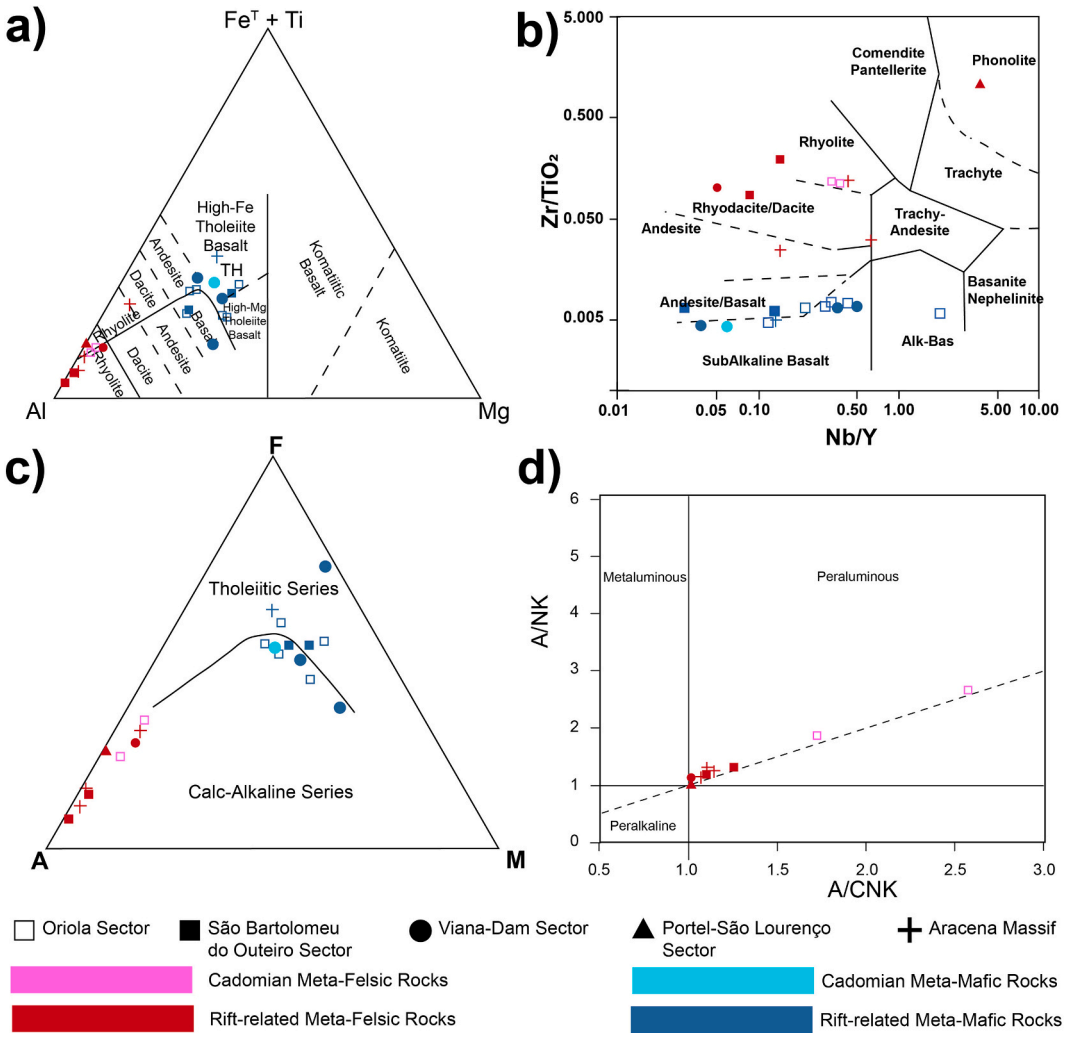

Appendix 1. – Geochemical classification diagrams of mafic and felsic samples: a) Jensen (1976) classification diagram; b) Winchester and Floyd (1977) classification diagram; c) AFM diagram by Irvine and Baragar (1971); and d) aluminosity index by Maniar and Piccoli (1989).

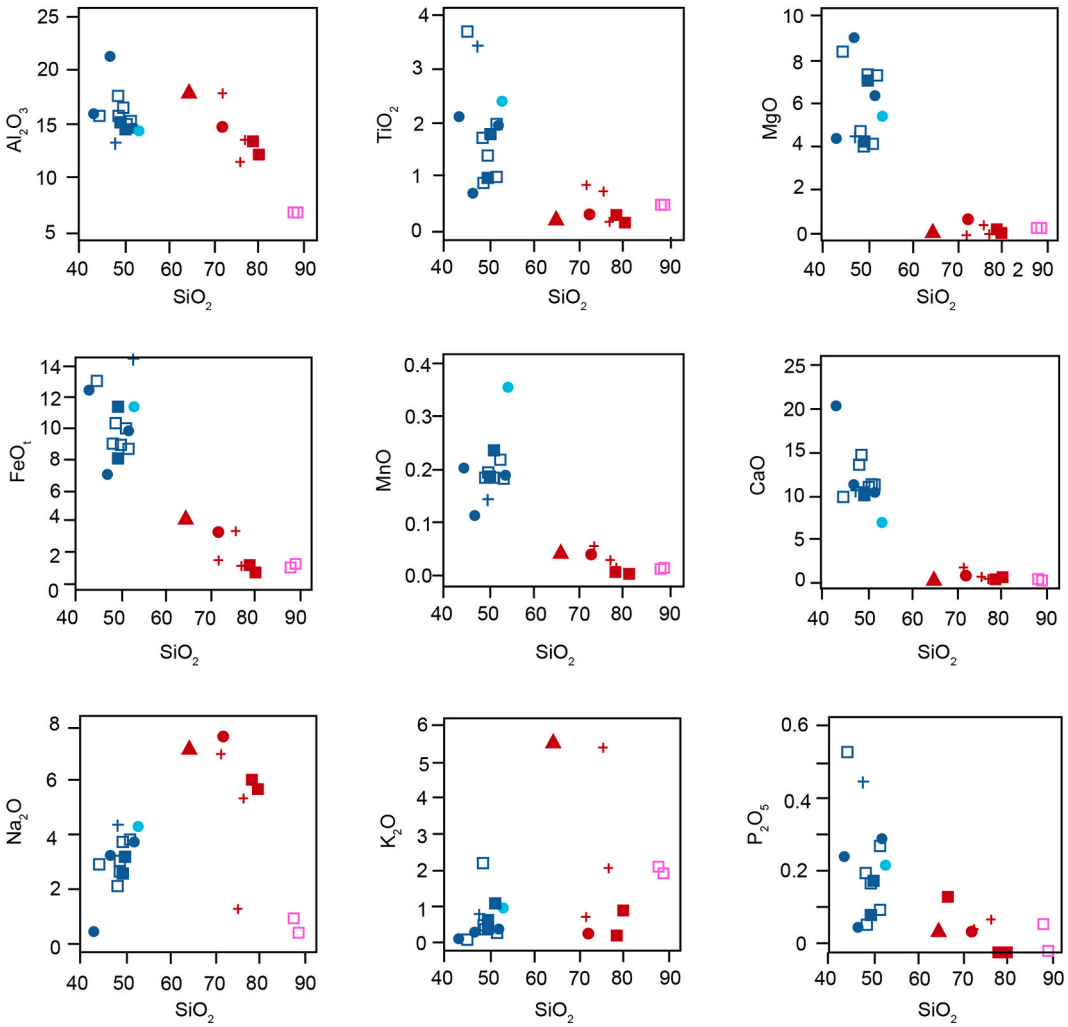

Appendix 2. – Harker diagrams for major elements of the studied meta-mafic and meta-felsic samples.

Appendix B. Supplementary data

Supplementary data to this article can be found online at https://doi.org/10.1016/j.chemer.2025.126351.

References

Ábalos, B.V., Gil Ibarguchi, I., Eguíluz, L., 1991. Structural and metamorphic evolution of the Almaden de la Plata Core (Seville, Spain) in relation to syn-metamorphic shear between the Ossa-Morena and south Portuguese zones of the Iberian Variscan fold belt. Tectonophysics 191 (3–4), 365–387. https://doi.org/10.1016/0040-1951(91)90068-4.

Akker, I.V., Tajčmanová, L., Marques, F.O., Burg, J.P., 2020. U–Pb zircon geochronology and phase equilibria modelling of HP-LT rocks in the Ossa-Morena Zone, Portugal. Int. J. Earth Sci. 109, 2719–2738. https://doi.org/10.1007/s00531-020-01921-w.

Araújo, A., Fonseca, P., Munhá, J., Moita, P., Pedro, J., Ribeiro, A., 2005. The Moura Phyllonitic complex: an accretionary complex related with Obduction in the southern Iberia Variscan suture. Geodin. Acta 18 (5), 375–388. https://doi.org/10.3166/ga.18.375-388.

Arenas, R., Martínez Catalán, J., Sánchez Martínez, S., Fernández-Suárez, J., Andonaegui, P., Pearce, J., Corfu, F., 2007. The Vila de cruces ophiolite: a remnant of the early Rheic Ocean in the Variscan suture of Galicia (northwest Iberian massif). J. Geol. 115 (2), 129–148. https://doi.org/10.1086/510645.

Bard, J.P., 1969. Le métamorphisme regional progressif de Sierra de Aracena en Andalousie occidentale (Espagne). PhD thesis, 397 p. Universite de Montpellier, France.

Bento dos Santos, T., Munhá, J., Tassinari, C., Fonseca, P., 2011. The link between partial melting, granitization and granulite development in Central Ribeira Fold Belt, SE Brazil: new evidence from elemental and Sr-Nd isotopic geochemistry. J. S. Am. Earth Sci. 31, 2–3. https://doi.org/10.1016/j.jsames.2011.01.004.

Bento dos Santos, T., Tassinari, C.C.G., Fonseca, P.E., 2015. Diachronic collision, slab break-off and long-term high thermal flux in the Brasiliano - Pan-African orogeny: implications for the geodynamic evolution of the Mantiqueira Province. Precambrian Res. 260, 1–22. https://doi.org/10.1016/j.precamres.2014.12.018.

Black, R., Latouche, L., Liégeois, J.P., Caby, R., Bertrand, J.M., 1994. Pan-African displaced terranes in the Tuareg shield (Central Sahara). Geology 22, 641–644. https://doi.org/10.1130/0091-7613(1994)022<0641:PADTIT>2.3.CO;2.

Brueseke, M., Hart, W.K., 2009. Intermediate composition magma production in an intracontinental setting: unusual Andesites and Dacites of the mid-Miocene Santa Rosa-calico volcanic field, northern Nevada. J. Volcanol. Geotherm. Res. https://doi.org/10.1016/j.jvolgeores.2008.12.015.

Bühn, B., Pimentel, M.M., Matteini, M., Dantas, E.L., 2009. High spatial resolution analysis of Pb and U isotopes for geochronology by laser ablation multi-collector inductively coupled plasma mass spectrometry (LA-MC-ICP-MS). An. Acad. Bras. Cienc. 81, 99–114. https://doi.org/10.1590/s0001-37652009000100011.

Cachapuz, P., Chichorro, M., Bento dos Santos, T., 2024. Critical analysis between the Ossa-Morena zone and the Galicia-Trás-Os-Montes zone, Iberian massif: geochemical and geochronological comparison and geodynamic implications. Geochemistry 84 (3), 126168. https://doi.org/10.1016/j.chemer.2024.126168.

Carrilho Lopes, J.M., 2004. Petrologia e geoquímica de complexos plutónicos do NE alentejano (Z.O.M.), Portugal central - Província alcalina e maciço de Campo Maior. PhD Thesis.. Universidade de Évora, Évora, Portugal, p. 526.

Carvalhosa, A., Zbyszewski, G., 1994. Notícia explicativa da folha 35-D: Montemor-o-Novo: Escala 1: 50.000. Serviços Geológicos de Portugal. 87p.

Castro, A., Fernández, C., De la Rosa, J., Moreno-Ventas, I., Rogers, G., 1996. Significance of MORB-derived Amphibolites from the Aracena Metamorphic Belt,

Southwest Spain. J. Petrol. 37 (2), 235–260. https://doi.org/10.1093/petrology/37.2.235.
Chichorro, M., Pereira, M.F., Díaz-Azpiroz, M., Williams, I.S., Fernández, C., Pin, C., Silva, J.B., 2008. Cambrian Ensialic rift-related magmatism in the Ossa-Morena zone (Évora-Aracena Metamorphic Belt, SW Iberian massif): Sm-Nd isotopes and SHRIMP zircon U-Th-Pb geochronology. Tectonophysics 461 (1–4), 91–113. https://doi.org/10.1016/j.tecto.2008.01.008.
Chichorro, M., Solá, A.R., Bento dos Santos, T.M., Lains Amaral, J., Crispim, L., 2022. Cadomian/Pan-African consolidation of the Iberian massif assessed by its detrital and inherited zircon populations: is the ~610Ma age peak a persistent Cadomian magmatic inheritance or the key to unravel its Pan-African basement? Geol. Acta 20 (15), 1–29. https://doi.org/10.1344/geologicaacta2022.20.15.
Condie, K.C., 2002. Breakup of a Paleoproterozoic supercontinent. Gondwana Res. 5, 41–43. https://doi.org/10.1016/S1342-937X(05)70886-8.
Cotrim, B., Bento dos Santos, T., Mata, J., Benoit, M., Jesus, A.P., 2021. Lower Paleozoic rifting event in central Iberian zone (central-North Portugal): evidence from elemental and isotopic geochemistry of metabasic rocks. Geochemistry 81 (3), 125768. https://doi.org/10.1016/j.chemer.2021.125768.
Crowley, Q., Winchester, J.A., Franke, W., Holland, J.G., 2000. Early Palaeozoic rift-related magmatism in Variscan Europe: fragmentation of the Armorican terrane assemblage. Terra Nova 12 (4). https://doi.org/10.1046/j.1365-3121.2000.00290.x.
DePaolo, D.J., Wasserburg, G.J., 1979. Sm-Nd age of the Stillwater complex and the mantle evolution curve for neodymium. Geochim. Cosmochim. Acta 43 (7), 999–1008. https://doi.org/10.1016/0016-7037(79)90089-9.
Díaz-Azpiroz, M., Castro, A., Fernández, C., López, S., Fernández Caliani, J.C., Moreno-Ventas, I., 2004. The contact between the Ossa Morena and south Portuguese zones. Characteristics and significance of the Aracena metamorphic belt, in its central sector between Aroche and Aracena (Huelva). J. Iber. Geol. 30, 23–51.
Díaz-Azpiroz, M., Fernandez, C., Castro, A., El-Biad, M., 2006. Tectonometamorphic evolution of the Aracena metamorphic belt (SW Spain) resulting from ridge-trench interaction during Variscan plate convergence. Tectonics 25 (1–20), TC1001. https://doi.org/10.1029/2004TC001742.
Díez-Fernández, R., Pereira, M.F., Foster, D.A., 2014. Peralkaline and alkaline magmatism of the Ossa-Morena zone (SW Iberia): age, source, and implications for the Paleozoic evolution of Gondwanan. Lithosphere 7 (1), 73–90. https://doi.org/10.1130/L379.1.
D'Lemos, R.S., Strachan, R.A., Topley, C.G., 1990. The Cadomian orogeny in the north Armorican massif: a brief review. Geol. Soc. Lond. Spec. Publ. 51 (1), 3–12. https://doi.org/10.1144/gsl.sp.1990.051.01.01.
Dostal, J., Patočka, F., Pin, C., 2001. Middle/late Cambrian intracontinental rifting in the central west Sudetes, NE bohemian massif (Czech Republic): geochemistry and petrogenesis of the bimodal meta-volcanic rocks. Geol. J. 36 (1), 1–17. https://doi.org/10.1002/gj.872.
Eguíluz, L., 1987. Petrogénesis de rocas ígneas y metamórficas en el Antiforme Burguillos-Monesterio, Macizo Ibérico meridional. PhD Thesis,. Univ. País Vasco, Spain, pp. 1–456.
Eguíluz, L., Ibarguchi, J.I.G., Abalos, B., Apraiz, A., 2000. Superposed Hercynian and Cadomian orogenic cycles in the Ossa-Morena zone and related areas of the Iberian massif. GSA Bull. 112 (9), 1398–1413. https://doi.org/10.1130/0016-7606(2000)112<1398:SHACOC>2.0.CO;2.
Ferreira, J.A., Pereira, I., Bento dos Santos, T., Mata, J., 2022. U-Pb age constraints on the source, cooling and exhumation of a Variscan middle crust migmatite complex from the central Iberian zone: insights into the Variscan metamorphic evolution and Ediacaran paleogeographic implications. J. Geol. Soc. Lond. 179 (5), 1–20. https://doi.org/10.1144/jgs2021-072.
Ferreira, P.L., Piçarra, J. (Coords.), 2020. Folha 6 da Carta Geológica de Portugal à escala 1:200 000. 1ª Edição, Laboratório Nacional de Energia, Lisboa. ISBN: 978-989-675-074-9.
Fitzsimons, I.C.W., 2000. Grenville-age basement provinces in East Antarctica: evidence for three separate collisional orogens. Geology 28, 879–882. https://doi.org/10.1130/0091-7613(2000)28<879:GBPIEA>2.0.CO;2.
Frei, D., Gerdes, A., 2009. Precise and accurate in situ U–Pb dating of zircon with high sample throughput by automated LA-SF-ICP-MS. Chem. Geol. 261 (3–4), 261–270. https://doi.org/10.1016/j.chemgeo.2008.07.025.
Giese, U., Walter, R., von Winterfeld, C., 1994. Geology of the southern Iberian Meseta II. The Aracena Metamorphic Belt between Almonaster La Real and Valdelarco, Huelva province (SW Spain). Neues Jb. Geol. Paläontol. Abh. 192, 333–360. https://doi.org/10.1127/njgpa/192/1994/333.
Gomes, E., Fonseca, P., 2006. Eventos Metamórfico/Metassomáticos Tardi-Variscos Na Região de Alvito (Alentejo, Sul de Portugal). Cadernos Do Laboratorio Xeoloxico de Laxe 31 (31), 67–85, 77.
Hajná, J., Žák, J., Dörr, W., Kachlík, V., Sláma, J., 2018. New constraints from detrital zircon ages on prolonged, multiphase transition from the Cadomian accretionary Orogen to a passive margin of Gondwana. Precambrian Res. 317, 159–178. https://doi.org/10.1016/j.precamres.2018.08.013.
Henriques, S., 2013. Magmatitos e Metamorfitos de Alto Grau No Contacto Entre as Zonas de Ossa Morena e Centro Ibérica: Significado Geodinâmico. Unpublished PhD Thesis.. Universidade de Coimbra.
Irvine, T., Baragar, W., 1971. A guide to the chemical classification of the common volcanic rocks. Can. J. Earth Sci. 8 (5), 523–548. https://doi.org/10.1139/e71-055.
Jackson, S.E., Pearson, N.J., Griffin, W.L., Belousova, E.A., 2004. The application of laser ablation-inductively coupled plasma-mass spectrometry to in situ U-Pb zircon geochronology. Chem. Geol. 211, 47–69.
Javier Álvaro, J., Bellido, F., Gasquet, D., Pereira, M.F., Quesada, C., Sánchez-García, T., 2014. Diachronism in the late Neoproterozoic–Cambrian arc-rift transition of North Gondwana: a comparison of Morocco and the Iberian Ossa-Morena Zone. J. Afr. Earth Sci. 98, 113–132. https://doi.org/10.1016/j.jafrearsci.2014.03.024.
Javier Álvaro, J., Sánchez-García, T., Casas, J.M., 2024. The Cambrian atlas – Ossa-Morena – Northarmorican rift, West Gondwana: Along- and off-axis, stratigraphic and volcano-tectonic patterns. In: Nance, R.D., Strachan, R.A., Quesada, C., Lin, S. (Eds.), Supercontinents. Geological Society, London, Special Publications, Orogenesis and Magmatism, p. 542. https://doi.org/10.1144/SP542-2023-24.
Jensen, L., 1976. A New Cation Plot for Classifying Subalkalic Volcanic Rocks, vol. 66. Ministry of Natural Resources.
Lemoine, S., Tempier, P., Bassot, J.P., Caen-Vachette, M., Vialette, Y., Toure, S., Wenmenga, U., 1990. The Burkinian orogenic cycle, precursor of the Eburnian orogeny in West Africa. Geol. J. 25 (2), 171–188. https://doi.org/10.1002/gj.3350250208.
Li, C., Li, X., Li, Q., Guo, J., Li, X., Yang, Y., 2012. Rapid and precise determination of Sr and Nd isotopic ratios in geological samples from the same filament loading by thermal ionization mass spectrometry employing a single-step separation scheme. Anal. Chim. Acta 727, 54–60. https://doi.org/10.1016/j.aca.2012.03.040.
Liew, T.C., Hofmann, A.W., 1988. Precambrian crustal components, plutonic associations, plate environment of the Hercynian Fold Belt of Central Europe: indications from a Nd and Sr isotopic study. Contrib. Mineral. Petrol. 98, 129–138. https://doi.org/10.1007/BF00402106.
Linnemann, U., Gehmlich, M., Tichomirowa, M., Buschmann, B., Nasdala, L., Jonas, P., et al., 2000. From Cadomian subduction to early Palaeozoic rifting: the evolution of Saxo-Thuringia at the margin of Gondwana in the light of single zircon geochronology and basin development (central European Variscides, Germany). Geol. Soc. Lond. Spec. Publ. 179 (1), 131–153. https://doi.org/10.1144/gsl.sp.2000.179.01.10.
Linnemann, U., Gerdes, A., Drost, K., Buschmann, B., 2007. The continuum between Cadomian orogenesis and opening of the Rheic Ocean: Constraints from LA-ICP-MS U–Pb zircon dating and analysis of plate-tectonic setting (Saxo-Thuringian zone, northeastern Bohemian Massif, Germany). In: Linnemann, U., Nance, R.D., Kraft, P., Zulauf, G. (Eds.), The evolution of the Rheic Ocean: From Avalonian-Cadomian active margin to Alleghenian-Variscan collision, 423. Geological Society of America Special Paper, pp. 61–96. https://doi.org/10.1130/2007.2423(03.
Linnemann, U., D'Lemos, R., Drost, K., Jeffries, T., Gerdes, A., Romer, R.L., Samson, S.D., Strachan, R.A., 2008a. Cadomian tectonics. In: McCann, T. (Ed.), The Geology of Central Europe. : Precambrian and Palaeozoic, vol. 1. The Geological Society of London, pp. 103–154. https://doi.org/10.1144/cev1p.3.
Linnemann, U., Pereira, M.F., Jeffries, T.E., Drost, K., Gerdes, A., 2008b. The Cadomian orogeny and the opening of the Rheic Ocean: the diacrony of geotectonic processes constrained by LA-ICP-MS U-Pb zircon dating (Ossa-Morena and Saxo-Thuringian zones, Iberian and bohemian massifs). Tectonophysics 461 (1–4), 21–43. https://doi.org/10.1016/j.tecto.2008.05.002.
Lugmair, G.W., Marti, K., 1978. Lunar initial 143Nd/144Nd: differential evolution of the lunar crust and mantle. Earth Planet. Sci. Lett. 39 (3), 349–357. https://doi.org/10.1016/0012-821X(78)90021-3.
Maniar, P., Piccoli, P., 1989. Tectonic discrimination of Granitoids. Geol. Soc. Am. Bull. 101 (5), 635–643. https://doi.org/10.1130/0016-7606(1989)101<0635:TDOG>2.3.CO;2.
Mata, J., Munha, J., 1986. Geodynamic Significance of High-Grade Metamorphic Rocks from Degolados-Campo Maior (Tomar-Badajoz-Córdoba Shear Zone). Maleo 2, 13, 28.
Mata, J., Munha, J., 1990. Magmatogénese de Metavulcanitos Câmbricos Do Nordeste Alentejano: Os Estádios Iniciais de" Rifting" Continental. Comunicações Dos Serviços Geológicos de Portugal 76, 61–89.
Mazzarini, F., Corti, G., Manetti, P., Innocenti, F., 2004. Strain rate and bimodal volcanism in the continental rift: Debre Zeyt volcanic field, northern MER. Ethiopia. Journal of African Earth Sciences 39 (3–5), 415–420. https://doi.org/10.1016/j.jafrearsci.2004.07.025.
McDonough, W.F., Sun, S., 1995. The composition of the earth. Chem. Geol. 120 (3–4), 223–253. https://doi.org/10.1016/0009-2541(94)00140-4.
Meert, J.G., 2001. Growing Gondwana and refining Rodinia: a paleomagnetic perspective. Gondwana Res. 4, 279–288. https://doi.org/10.1016/S1342-937X(05)70329-4.
Moita, P., Santos, J.F., Pereira, M.F., Costa, M.M., Corfu, F., 2015. The quartz-dioritic Hospitais intrusion (SW Iberian massif) and its mafic microgranular enclaves—evidence for mineral clustering. Lithos 224, 78–100. https://doi.org/10.1016/j.lithos.2015.02.012.
Moreira, N., 2017. Evolução Geodinâmica Dos Sectores Setentrionais Da Zona de Ossa-Morena No Contexto Do Varisco Ibérico. Unpublished PhD Thesis.. Universidade de Évora.
Moreno-Eiris, E., 1987. Los montículos arrecifales de algas y arqueociatos del Cámbrico Inferior de Sierra Morena. Publicaciones especiales del Boletín Geológico y Minero 98, 1–127.
Moreno-Martín, D., Díez Fernández, R., Arenas, R., Rojo-Pérez, E., Novo-Fernández, I., Sánchez Martínez, S., 2023. Building and collapse of the Cadomian Orogen: a plate-scale model based on structural data from the SW Iberian massif. Tectonics 42 (12), e2023TC007990. https://doi.org/10.1029/2023TC007990.
Murphy, J.B., Eguiluz, L., Zulauf, G., 2002. Cadomian orogens, peri-gondwanan correlatives and laurentia–baltica connections. Tectonophysics 352, 1–9. https://doi.org/10.1016/S0040-1951(02)00186-5.
Murphy, J.B., Keppie, J.D., Nance, R.D., Miller, B.V., Dostal, J., Middleton, M., Fernandez-Suarez, J., Jefferies, T.E., Storey, C.D., 2006. Geochemistry and U–Pb protolith ages of eclogitic rocks of the Asis Lithodeme, Piaxtla Suite, Acatlán Complex, southern Mexico: tectonothermal activity along the southern margin of the

Rheic Ocean. J. Geol. Soc. Lond. 163 (4), 683–695. https://doi.org/10.1144/0016-764905-108.
Nance, R.D., Miller, B.V., Keppie, J.D., Murphy, J.B., Dostal, J., 2006. The Acatlán complex, southern Mexico: record of Pangea assembly to breakup. Geology 34, 857–860. https://doi.org/10.1130/0091-7613(1999)027<0099:SCOALB>2.3.CO;2.
Nance, R.D., Murphy, J.B., Strachan, R.A., Keppie, J.D., Gutierrez-Alonso, G., Fernandez-Suarez, J., Quesada, C., Linnemann, U., D'Lemos, R., Pisarevsky, S.A., 2008. Neoproterozoic-early Paleozoic tectonostratigraphy and palaeogeography of the peri-Gondwanan terranes: Amazonian v. West African connections. In: Ennih, N., Liegeois, J.-P. (Eds.), The Boundaries of the West African Craton, 297. Geological Society of London Special Publication, p. 345e383. https://doi.org/10.1144/SP297.17.
Oliveira, J.T., Oliveira, V., Piçarra, J.M., 1991. Traços Gerais Da Evolução Tectono-Estratigráfica Da Zona de Ossa-Morena, Em Portugal. In: Comunicações Dos Serviços Geológicos de Portugal, 77, pp. 3–26. Fevereiro 2016.
Padel, M., Javier Álvaro, J., Casas, J.M., Clausen, S., Poujol, M., Sánchez-García, T., 2018. Cadomian volcanosedimentary complexes across the Ediacaran–Cambrian transition of the Eastern Pyrenees, southwestern Europe. Int. J. Earth Sci. 107, 1579–1601. https://doi.org/10.1007/S00531-017-1559-5.
Pearce, J.A., 1982. Trace element characteristics of lavas from destructive plate boundaries. In: Thorpe, R.S. (Ed.), Andesites, orogenic andesites and related rocks. Wiley, Chichester, pp. 525–548.
Pearce, J., 2008. Geochemical fingerprinting of oceanic basalts with applications to ophiolite classification and the search for Archean oceanic crust. Lithos 100 (1–4), 14–48. https://doi.org/10.1016/j.lithos.2007.06.016.
Pearce, J., Harris, N., Tindle, A., 1984. Trace element discrimination diagrams for the tectonic interpretation of granitic rocks. J. Petrol. https://doi.org/10.1093/petrology/25.4.956.
Pedro, J., Araújo, A., Fonseca, P., Tassinari, C., Ribeiro, A., 2010. Geochemistry and U-Pb zircon age of the internal Ossa-Morena zone ophiolite sequences: a remnant of Rheic Ocean in SW Iberia. Ofioliti. https://doi.org/10.4454/ofioliti.v35i2.390.
Pereira, M.F., Silva, J.B., Chichorro, M., 2003. Internal structure of the Évora high-grade terrains and the Montemor-o-Novo shear zone. Geogaceta. Sociedad Geologica de Espana 33, 79–82.
Pereira, M.F., Chichorro, M., Williams, I., Silva, J.B., Fernández, C., Díaz-Azpíroz, M., Apraiz, M., Castro, A., 2009. Variscan intra-orogenic extensional tectonics in the Ossa-Morena zone (Évora-Aracena-Lora Del Río Metamorphic Belt, SW Iberian massif): SHRIMP zircon U-Th-Pb geochronology. Geol. Soc. Lond. Spec. Publ. 327, 215–237. https://doi.org/10.1144/SP327.11.
Pereira, M.F., Gama, C., da Silva, I.D., Fuenlabrada, J.M., El Houicha, M., 2023. Cadomian arc recycling along the northern Gondwana margin: source-inherited composition of Miaolingian rift-related rhyolitic rocks (Ossa-Morena zone, SW Iberia). J. Afr. Earth Sci. 201, 104887. https://doi.org/10.1016/j.jafrearsci.2023.104887.
Petrinovic, I.A., Riller, U., Brod, J.A., Alvarado, G., Arnosio, M., 2006. Bimodal volcanism in a tectonic transfer zone: evidence for tectonically controlled magmatism in the southern Central Andes, NW Argentina. J. Volcanol. Geotherm. Res. 152 (3–4), 240–252. https://doi.org/10.1016/j.jvolgeores.2005.10.008.
Piçarra, J., 2000. Estudo Estratigráfico Do Sector de Estremoz-Barrancos, Zona de Ossa-Morena. Portugal. Unpublished PhD thesis.. Universidade de Évora, p. 268.
Quesada, C., Apalategui, O., Eguíluz, L., Liñan, E., Palacios, T., 1990. Stratigraphy of Ossa - Morena zone: pre-Cambrian. In Pre-Mesozoic Geology of Iberia 252–258.
Rosas, F.M., Marques, F.O., Ballevre, M., Tassinari, C., 2008. Geodynamic evolution of the SW Variscides: orogenic collapse shown by new tectonometamorphic and isotopic data from western Ossa-Morena zone, SW Iberia. Tectonics 27 (6). https://doi.org/10.1029/2008TC002333.
Sánchez-García, T., Bellido, F., Quesada, C., 2003. Geodynamic setting and geochemical signatures of Cambrian-Ordovician rift-related igneous rocks (Ossa-Morena zone, SW Iberia). Tectonophysics 365 (1–4), 233–255. https://doi.org/10.1016/S0040-1951(03)00024-6.
Sánchez-García, T., Bellido, F., Pereira, M.F., López-Guijarro, R., Quesada, C., Chichorro, M., Silva, J.B., Pin, C., 2008. Expresión magmática temprana de un rift intracontinental en el margen de Gondwana durante el Cámbrico Inferior: Zona de Ossa-Morena (SW Macizo Ibérico, Portugal, España). Geo-Temas 10, 1567–1572.
Sánchez-García, T., Bellido, F., Pereira, M.F., Chichorro, M., Quesada, C., Pin, C., Silva, J. B., 2010. Rift-related volcanism predating the birth of the Rheic Ocean (Ossa-Morena zone, SW Iberia). Gondwana Res. 17 (2–3), 392–407. https://doi.org/10.1016/j.gr.2009.10.005.
Sánchez-García, T., Pereira, M.F., Bellido, F., Chichorro, M., Silva, J.B., Valverde-Vaquero, P., Pin, C., Solá, A.R., 2014. Early Cambrian Granitoids of North Gondwana margin in the transition from a convergent setting to intra-continental rifting (Ossa-Morena zone, SW Iberia). Int. J. Earth Sci. 103 (5). https://doi.org/10.1007/s00531-013-0939-8.
Sánchez-García, T., Chichorro, M., Solá, A.R., Álvaro, J., Díez-Montes .F., A., Bellido, F., Ribeiro, M.L., Quesada, C., Lopes, J.C., Dias da Silva, Í., González-Clavijo, E., Gómez Barreiro, J., López-Carmona, A., 2019. The Cambrian-early Ordovician rift stage in the Gondwanan units of the Iberian massif. In. https://doi.org/10.1007/978-3-030-10519-8_2.
Sánchez-Lorda, M.E., Sarrionandia, F., Ábalos, B., Carracedo, M., Eguiluz, L., Gil Ibarbuchi, J.I., 2014. Geochemistry and paleotectonic setting of Ediacaran metabasites from the Ossa-Morena Zone (SW Iberia). Int. J. Earth Sci. 103, 1263–1286.
Sánchez-Lorda, M.E., Ábalos, B., García de Madinabeitia, S., Eguiluz, L., Gil Ibarguchi, J. I., Paquette, J.L., 2016. Radiometric discrimination of pre-Variscan amphibolites in the Ediacaran Serie Negra (Ossa- Morena zone, SW Iberia). Tectonophysics 681, 3145. https://doi.org/10.1016/j.tecto.2015.09.020.
Shinjo, R., Kato, Y., 2000. Geochemical constraints on the origin of bimodal magmatism at the Okinawa trough, an incipient back-arc basin. Lithos 54 (3–4), 117–137. https://doi.org/10.1016/S0024-4937(00)00034-7.
Simancas, F., Expósito, I., Azor, A., Martínez Poyatos, D., González Lodeiro, F., 2004. From the Cadomian orogenesis to the early Palaeozoic Variscan rifting in Southwest Iberia. J. Iber. Geol. 30, 53–71.
Sláma, J., Košler, J., Condon, D.J., Crowley, J.L., Gerdes, A., Hanchar, J.M., Horstwood, M.S.A., Morris, G.A., Nasdala, L., Norberg, N., Schaltegger, U., Schoene, B., Tubrett, M.N., Whitehouse, M.J., 2008. Plešovice zircon—a new natural reference material for U–Pb and Hf isotopic microanalysis. Chem. Geol. 249 (1–2), 1–35. https://doi.org/10.1016/j.chemgeo.2007.11.005.
Stacey, J.S., Kramers, J.D., 1975. Approximation of terrestrial lead isotope evolution by a two-stage model. Earth Planet. Sci. Lett. 26, 207–221.
Taylor, S., McLennan, S., 1995. The geochemical evolution of the continental crust. Rev. Geophys. 33 (2), 241–265. https://doi.org/10.1029/95RG00262.
Vermeesch, P., 2018. IsoplotR: a free and open toolbox for geochronology. Geosci. Front. 9 (5), 1479–1493. https://doi.org/10.1016/j.gsf.2018.04.001.
Wilson, M., 1989. Igneous petrogenesis. Unwin Hyman, London.
Winchester, J.A., Floyd, P.A., 1977. Geochemical discrimination of different magma series and their differentiation products using immobile elements. Chem. Geol. 20, 325–343.
Winchester, J.A., Pharaoh, T.C., Verniers, J., Ioane, D., Seghedi, A., 2006. Palaeozoic accretion of Gondwana-derived terranes to the east European craton: recognition of detached terrane fragments dispersed after collision with promontories. Geol. Soc. Mem. 32. https://doi.org/10.1144/GSL.MEM.2006.032.01.19.
Wood, D.A., 1980. The application of a Th-Hf-ta diagram to problems of Tectonomagmatic British tertiary Volcanic Province. Earth Planet. Sci. Lett. 42, 77–97.